

Geochemical modelling of fluid-rock interaction in sandstones caused by sill emplacement using the NUFT code

Susanne Schmid & William Glassley



Geochemical modelling of fluid-rock interaction in sandstones caused by sill emplacement using the NUFT code

Susanne Schmid & William Glassley

Released 01.03.2012

Executive summary

This report is a supplement to the original report on the impact of Palaeogene sill emplacement on potential reservoir lithologies in East Greenland and Scotland. It represents the results of the geochemical modeling study and applies them to reservoir lithologies of the Faroe-Shetland Basin. This work was funded by the SINDRI Group.

The overall aim of this SINDRI project is to develop a model for predicting effects of sill emplacement on reservoir properties of sandstones, with particular relevance to understanding the influence of diagenetic processes on permeability and thermal evolution.

The effect of sill emplacement on shallow-buried sandstones varies significantly depending on (1) the detrital composition of the sandstones and (2) the temperature of the intrusion.

The detrital composition of the sandstone has an effect on (1) the compaction curve during burial and subsequently porosity changes and (2) the feasibility of cementation (e.g. clay coating prevents quartz cementation).

The results of the main report (Schmid, 2006) are: The temperature of the intrusion has an effect on (1) the solubility of quartz (quartz becomes more likely to dissolve with increasing temperatures) and subsequently quartz cementation, (2) the degree of clay mineral replacement resulting in permeability loss and (3) the extent of mineral alterations (e.g. metasomatism, albitisation and chloritisation).

The results of the geochemical modeling show that the temperature increase in the sediment due to sill emplacement has no significant impact on porosity. However, mineral dissolution and reprecipitation such as illitisation and K-feldspar dissolution occur. The geochemical modeling did not confirm the observed diagenetic changes in sandstones from Skye. The Skye samples have major quartz cementation (~8%), while the modelled results are below 1%. This implies that the temperature is not the overall control in mineral precipitation. Other variables such as pore connectivity and pressure due to sill emplacement must play a significant role too. Neither can be modelled using the NUFT code.

Therefore, it is suggested that the definition of the contact aureole should be distinguished between **chemical** contact aureole and **physical** contact aureole. The chemical or geochemical contact aureole defines the zone of geochemical changes (dissolution and precipitation of minerals) stimulated by heating and subsequent cooling. The modeling suggests a zone, which is half the width of the intrusion if the host sediment is homogeneous and mineral volume and porosity changes are below 1%. The physical contact aureole defines the zone of physical changes (compaction (porosity loss of 15%), fracturing and grain rearrangement) caused by space generation and pressure changes during emplacement. The width of the physical aureole in homogeneous sediments varies depending on thickness of the intrusion and overburden during emplacement. Significant cementation (~8% quartz) and reduction of porosity (8-9%) and permeability (1 Md) can only occur in the zone where physical and chemical contact aureoles overlap.

Content

Introduction	4
Project Aims	5
Geochemical modeling	6
Introduction	6
Methods	7
Simulation setup.....	8
Simulation series.....	9
Rock, mineral and fluid properties.....	10
Results	14
Interpretation	25
Heating processes.....	26
Cooling processes.....	26
Porosity changes.....	27
Mineral abundance changes	27
Comparison with Skye data	28
Conclusion	30
Acknowledgments	32
References	33
Appendix	34

Introduction

The Faroe-Shetland Basin potential reservoir rocks are intruded by sills and overlain by thick basaltic extrusive rocks. The impact of these intrusions on reservoir maturation, heat flow and reservoir properties are widely unknown.

The SINDRI group has initiated the project on the impact of Palaeogene sill emplacement on reservoir lithologies in East Greenland and the Faroe-Shetland Basin. The studies on two onshore, outcrop analogues were undertaken on the Isle of Skye (Scotland) and Traill Ø (East Greenland) with the goal to petrographically describe the contact rock and define the contact diagenetic changes, simulate the intrusive event in a geochemical computer model and predict the impact of sill emplacement in the Faroe-Shetland Basin sediment properties.

This report presents the geochemical modeling results and interpretation of thermal effects of sill emplacement on sandstones. The data are derived from a computer simulated model using the NUFT code.

Project Aims

This report presents the results of a geochemical modeling study and replaces that part in the main report on "Impact of Palaeogene sill emplacement on potential reservoir lithologies in East Greenland and the Faroe-Shetland Basin" (Schmid, 2006).

The overall aim of the project is to develop a model for predicting the effects of sill emplacement on reservoir properties of sandstones.

The specific aim of this part of the project is:

1. Quantitative modeling of coupled thermally driven fluid-flow and fluid-rock geochemical interactions in reservoir lithologies relating to sill emplacement and correlation with regional models.

Further aims that were part of the main report (Schmid, 2006) are:

2. Constraining mineralogical effects of sill emplacement on adjacent sandstones.
3. Constraining the relationship between sill proximity and sandstone porosity and permeability.

Geochemical modeling

Introduction

Geochemical modeling must cover two aspects in order to achieve a quantitative prediction of mineral reactions – geochemical and hydrodynamic processes. Geochemical processes include aqueous speciation and redox reactions, interface reactions, precipitation and dissolution of minerals and colloids. Hydrodynamic transport processes include diffusion and migration due to advective forces, leading to dispersion of the chemical species in space and time (Kuehn, 2004). Geological processes such as diagenesis, hydrothermal ore deposit formation and metamorphism are the result of reactive transport in the subsurface. Chemical changes are driven by the interaction between migrating fluids and solid phases while fluid flow, heat transfer, solute transport and time influence the evolution of these systems. Hydrogeochemical or non-reactive fluid flow models have been the centre of much controversy concerning the validity and uncertainties of the model input (Konikow & Bredehoeft, 1992).

Within the last five years it has become possible to rigorously simulate the chemical interaction between fluid and rock, taking into account the effects of varying temperature, porosity/permeability evolution and fluid flow. This coupled system has been understood, in principle, for more than thirty years, but the computational tools to construct numerical models of such systems was not possible until massively parallel computers, in which hundreds or thousands of processors are linked, became available. Such simulations can now be done at high resolution in three dimensions, allowing the study of evolving permeability and mineralogy, and fluid migration, as physical conditions change over geological time. These simulations, however, can require weeks to months of time on such machines, if the systems under consideration are chemically or hydrologically complex. Access to massively parallel computers, however, is very limited. As a result, it has proven to be useful to adapt these simulation tools to work station computers, thus allowing modeling of these thermo-hydrological – geochemical systems by anyone in the geological community. Work station-based simulations are a powerful means to explore the behaviour of evolving geological systems. But, because of the diminished computational power available on these platforms, such simulations are subject to several challenges.

Foremost is the challenge of establishing the appropriate computer code control parameter values that suitably represent the system being studied. The numerical problem being undertaken in these simulations is “stiff”. In mathematics, a “stiff” equation is a differential equation for which numerical methods for solving the equation are numerically unstable. This reflects the fact that the equation being solved includes some terms that can lead to rapid variation in the solution. The step size and convergence tolerances stipulated for solving the equation are usually determined simply through trial and error, and experience. In the problem being solved in coupled flow and transport systems, there are many nonlinearly coupled partial differential equations that must be solved simultaneously. This multiplicity of equations profoundly increases the difficulty of stipulating the right set of solver parameters that will allow efficient solution of the mathematical problem. Only through patient trial and error of stipulating convergence tolerances for the linear and nonlinear

solvers can reasonable estimates be made of the initial conditions for beginning the simulations.

Once the challenge of getting the code to run well has been met, the next most significant challenge is developing the actual values of the physical and chemical parameters necessary to realistically represent the specific system being studied. Most geological systems in which a pore fluid is present have evolved over millions of years. The chemical composition of the pore fluid will reflect complex interactions that are controlled by the local mineralogy on the pore scale, as well as local variations in pressure and temperature, composition of dissolved gases, and other intensive and extensive variables. A simulation or series of simulations are then run that allow the system to “condition” itself, meaning it is allowed to evolve over thousands of years to reach steady-state conditions that reflect the effects of gradients in temperature, pressure, flow field, chemistry or mineralogy. These “conditioned” values are then used as the initial or starting point values in later simulations that are intended to model the actual evolution of the system.

Finally, once the code control parameters and initial geological system parameters are established, numerous simulations are then required to evaluate how the system evolves through time, for the given set of perturbations or evolutionary changes imposed on it. This part of the task is important, in order to determine the extent to which the initial conceptual model realistically represented the time-dependent behaviour of the system, and whether small differences in the initial values of certain parameters can strongly affect the outcome (i.e., sensitivity studies). These simulations can allow clear description of the likely evolutionary pathway followed by a geological system, but they only have merit if it can be demonstrated that the solution is robust, meaning that numerous simulations have been conducted, most of which lend support, one way or another, to the conceptual model being described, and that other models are ruled out.

Computational modeling of heat and fluid flow in geochemical processes, including quantitative description of time-dependent evolution of porosity, permeability, mineralogy and fluid flow regimes driven by heat associated with emplacement of mafic intrusion into sediments was approached using the NUFT code developed by the Lawrence Livermore National Laboratory, USA.

In this project we set up several simulations with a fluid flow over a time period of 100.000 years in order to get an initial fluid. Further, parts of the sandstone get heated in order to see what happens between heated and non-heated intervals. And last, a sill composition and temperature next to the sandstone is simulated. All simulations are for the purpose of seeing how the fluid interacts with the minerals and how temperature effects fluid-rock interaction along the contact.

Methods

The NUFT (Non-isothermal Unsaturated-Saturated Flow and Transport model) is a suite of multi-phase, multicomponent models for numerical solution of non-isothermal flow and transport in porous media with application to subsurface transport problems. Models in the code allow simulations of unconfined and confined saturated flow, single-phase unsaturated flow, single-component contaminant transport, and multi-phase, multi-component flow and transport with non-isothermal conditions (Nitao, 1998). Latter was used for the sill emplacement simulations.

In more detail, the NUFT code is designed to rigorously model fluid and mass transport of multiple phases in porous media. Both diffusive and advective flow are considered and treated simultaneously. Fundamental conservation laws are treated explicitly, taking into account full conservation of mass, momentum and energy. Thus, flow in the porous media will occur in response to gradients in thermal, pressure, density or chemical conditions.

The initial physical properties of the media through which flow occurs are specified by the user (porosity, 3-dimensional permeability, heat capacity, connectivity, etc.). Boundary conditions are also specified, and can be time-varying. The physical properties of the porous media can be specified as fixed, in which case the initial and final conditions for flow are the same, or they can be allowed to evolve as mineral dissolution and/or precipitation occur. In the latter case, the porosity and permeability will change through time, and will modify the behavior of the flow field.

In the simulations conducted here, the physical properties of the porous media were allowed to evolve as mineral dissolution and precipitation occurred. Furthermore, the boundary conditions were specified such that the system was allowed to evolve as though it were an open system, which is consistent with the behavior of the geological system being modeled.

The NUFT code version 3.1 is running on a LINUX RedHat Operating System PC.

Simulation setup

The NUFT code presents the possibility to model fluid-rock interaction in x, y and z direction. The model is set up such that each direction can be given a number of cells. Each cell or numbers of cells can have specific rock properties (e.g. porosity, mineral composition and mineral abundance). The combination of all cells defines a 3D mesh. The simulations for this project have been set up such that the x and y directions contain 1 cell and the z direction has 36 cells and defines the depth (Fig. 1). Each cell was given the specific parameter of either sandstone or sill (specific parameters for each simulation are described in Simulation series). Cell number 0 is an initiation (boundary) cell and might not be used for data interpretation. Cells without neighbouring cells have a large error range in the simulations. The fluid was heated under a time and temperature controlled setting – meaning that heating and cooling took place in a timescale of years to thousands of years in order to later analyse e.g. mineral abundance changes or porosity at a certain time and temperature.

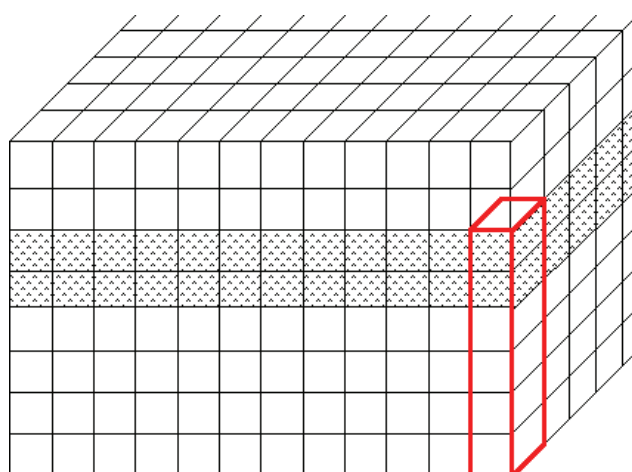


Figure 1. Schematic model of sill within sandstone (white boxes). Red marked area represents computational modelled cells.

Thermal perturbation of the system during sill emplacement is represented as a boundary condition by allowing a time-evolving temperature history for certain cells. Fluid flow and

mineral reactions occur in response to this thermal history. This approach is justified for these initial simulations because the rates of sill injection and wall rock heating are unknown, the initial magma temperature is unknown, and the duration of the heating period is unknown. These simulations, thus, are not intended to represent the exact behaviour of the natural system but instead provide insight into the general behavior that would be expected in the case of a thermal history as represented here. Once more rigorous knowledge is available regarding the actual thermal history experienced by the sediments as sill injection occurred, it would be appropriate to update these simulations with those thermal constraints.

Mineral dissolution and precipitation reactions are thermodynamically controlled processes that occur at measurable, but slow, rates. The direction of a reaction is determined by the intensive and extensive parameters that control reactions. The NUFT code evaluates the thermodynamic state of the fluid and its solute load at each time step, determines whether minerals are undersaturated, supersaturated or at equilibrium, and then applies a rate law to dissolve or precipitate the appropriate amount of a mineral phase at that time step. Thus, NUFT is not an equilibrium geochemical modeling code but a kinetic, reactive transport modeling code. This point is important because the time steps are controlled by the numerical constraints needed to assure accurate and precise solutions to the linear and non-linear equations involved in these complex systems. The time steps can be very small (fractions of a second), which is much too short a time for geological systems to achieve thermodynamic equilibrium; dissolution and precipitation rates are often on the order of 10^{-10} to 10^{-12} moles/m²-sec at temperatures less than 300°C. It is thus crucial that reaction rates be considered when conducting such modeling, rather than assuming that chemical equilibrium is achieved at each time step.

Simulation series

The simulations were extended from the original plan as presented in Schmid, 2006.

The simulations carried out successfully are:

1. Sandstone (quartzite) with porosity of 40%, temperature of 30°C, marine fluid and fluid-flow activated, simulated time 100.000 years
2. Sandstone (quartzite) with porosity of 25%, temperature of 90°C, marine fluid and fluid flow activated, simulated time 100.000 years
3. Sandstone (sample 110) with porosity of 25%, temperature of 90°C, neutral fluid and fluid flow activated, simulated time 10.000 years (inmod02)
4. Sandstone (sample 110) with porosity of 25%, temperature of 90°C, fluid from test 3 and fluid flow activated, simulated time 10.000 years (inmod04)
5. Sandstone (sample 110) with porosity of 18%, temperature of 120°C, fluid from test 4 and fluid flow activated, simulated time 10.000 years (inmod05)
6. Sandstone (sample 110) with porosity of 25%, temperature of 90°C, fluid from test 3 and fluid flow deactivated, simulated time 10.000 years (inmod08)
7. Sandstone (sample 110) with porosity of 25%, starting temperature of 90°C, heating up to 300°C and fluid flow activated, heated cells 9 out of 36, simulated time 10.000 years (test13)

8. Sandstone (sample 110) with porosity of 10% (cell 4-8) and 25% (cells 9-36) and sill (basalt CIPW-norm sample 101) with porosity of 3%, starting temperature of 90°C, heating up to 250°C, heated cells 1-3 out of 36, simulated time 10.000 years (test14) and fluid flow activated

All simulations were modelled in an open system. There have been more than 40 simulations with varying parameters of which the above gave realistic results.

Rock, mineral and fluid properties

Three different rock types have been used; (1) sandstone which consists of exclusively quartz, (2) sandstone that has the composition as in Skye sample 110 (Table 1; Schmid, 2006) and (3) a mineral composition close to basalt (Table 2).

Quartzite:

- 75% quartz
- 25% porosity

Sandstone sample 110 (slightly altered):

- albite 3.3%
- K-feldspar 3.62%
- montmorillonite 2%
- phlogopite 0.32%
- quartz 63.8%
- porosity 25%

The mineral abundance has been recalculated for the lower porosity simulations accordingly.

Basalt sample 101 (simplified):

- albite 27.33%
- K-feldspar (orthoclase) 3.01%
- quartz 1.47%
- porosity 3%

Anorthite, diopside, hypersthene, ilmenite, hematite, sphene and apatite have not been used for the simulation due to technical complications, but have no effect on the outcome of the modeling.

XRF data (wt%)

SiO2	TiO2	Al2O3	Fe2O3	MnO	MgO	CaO	Na2O	K2O	P2O5	Volat	FeO	Total
94.356	0.495	1.812	0.403	0.003	0.130	0.047	0.190	0.769	0.021	0.420	0.363	99.009

Modal analysis data

Detrital Mineralogy								Authigenic Mineralogy			Porosity	Total
Total Qtz	K-fsp	Plag	Musc.	Biotite	Frag.	Sed.	Heavy min.	Matrix clay	Chlorite	Qtz overg	Pyrite	
63,00	3,67	3,33	0,33	0,33	0,33	0,33	1,67	0,67	1,67	0,67	24,00	100,00
		<i>Albite</i>			<i>Rutile</i>		<i>Illite</i>					

Table 1. Initial sandstone composition (whole rock geochemistry and modal analysis data) from Skye sample 110 (Schmid, 2006).

CIPW-norm

Sample-ID	quartz	orthoclase	albite	anorthite	diopside	hypersthene	ilmenite	hematite	sphene	apatite	Sum
101	1.47	3.01	27.33	26.56	14.74	9.33	0.34	11.68	3.95	0.42	98.82

XRF data (wt%)

Sample_ID	SiO2	TiO2	Al2O3	Fe2O3	MnO	MgO	CaO	Na2O	K2O	P2O5	Volat	Sum,maj.
101	48,651	1,786	15,598	11,677	0,158	6,490	10,533	3,230	0,510	0,178	0,670	99,481

Table 2. Initial sill (basalt) composition (CIPW-norm calculated from whole rock geochemistry from Skye sample 101 (Schmid, 2006).

The mineral and phase composition has been adapted from JNCChem provided by William Glassley. The initial, simplified chemistry for Fe-free system (MolWt in g/mol) is specified below. “Solid-phases” refers to the minerals considered. “Basis-species” are the chemical components that compose the system. “Aux-basis-species” are all aqueous species that can occur in the fluid phase. “Solids and Minerals” is a tabulation of the properties for each solid phase (chemical formula, molecular weight, stoichiometry of the applicable hydrolysis reaction (negative coefficients indicate reactants, positive coefficients indicate products), and the rate constant for the dissolution and precipitation reactions (given in moles per square meter of surface area of the mineral per second):

Solid-phases:

- Albite-low
 - K-Feldspar
 - Montmorillonite-K (replacement for illite)
 - Phlogopite (replacement for biotite)
 - Quartz

Basis-species:

- H₂O (MoleWt 18.015)
 - H⁺ (MoleWt 1.008)
 - Al⁺⁺⁺ (MoleWt 26.982)
 - Ca⁺⁺ (MoleWt 40.078)
 - Cl⁻ (MoleWt 35.453)

- K⁺ (MoleWt 39.098)
- Mg⁺⁺ (MoleWt 24.305)
- Na⁺ (MoleWt 22.990)
- SiO₂_aq (MoleWt 60.084)
- air (MoleWt 29)

Aux-basis-species:

- H⁺ (MoleWt 1.008)
- OH⁻ (MoleWt 17.007)
- Al⁺⁺⁺ (MoleWt 26.982)
- AlO⁺ (MoleWt 42.981)
- Ca⁺⁺ (MoleWt 40.078)
- Cl⁻ (MoleWt 35.453)
- K⁺ (MoleWt 39.098)
- Mg⁺⁺ (MoleWt 24.305)
- Na⁺ (MoleWt 22.990)
- SiO₂²⁻_aq (MoleWt 60.084).

Solids and Minerals:

Albite_low	(NaAlSi ₃ O ₈) (MoleWt 262.223) (species Albite_low (-1.00) H ⁺ (-4.00) Al ⁺⁺⁺ (1.00) Na ⁺ (1.00) H ₂ O (2.00) SiO ₂ _aq (3.00)) (rateConstant 1.0e-14 at 25°C in mol/m**2/s)
K-Feldspar	(KAlSi ₃ O ₈) (MoleWt 278.332) (species K-Feldspar (-1.00) H ⁺ (-4.00) Al ⁺⁺⁺ (1.00) K ⁺ (1.00) H ₂ O (2.00) SiO ₂ _aq (3.00)) (rateConstant 1.0e-12 at 25°C in mol/m**2/s)
Montmorillonite-K	(K _{.33} Mg _{.33} Al _{1.67} Si ₄ O ₁₀ (OH) ₂) (MoleWt 372.333) (species Montmorillonite-K (-1.00) H ⁺ (-6.00) K ⁺ (0.33) Mg ⁺⁺ (0.33) Al ⁺⁺⁺ (1.67) SiO ₂ _aq (4.00) H ₂ O (4.00)) (rateConstant 5.2e-14 assumed equivalent to kaolinite at 25°C)
Phlogopite	(KAlMg ₃ Si ₃ O ₁₀ (OH) ₂) (MoleWt 417.260) (species Phlogopite (-1.00) H ⁺ (-10.00) Al ⁺⁺⁺ (1.00) K ⁺ (1.00) Mg ⁺⁺ (3.00) SiO ₂ _aq (3.00) H ₂ O (6.00)) (rateConstant 3.8e-13 at 25°C in mol/m**2/s)
Quartz	(SiO ₂) (MoleWt 60.084) (species Quartz (-1.00) SiO ₂ _aq (1.00))

(rateConstant 1.26e-14 at T25°C in mol/m**2/s)

The fluid properties vary with different simulations. Generally, the first initial fluid composition is a marine water or diluted fluid. The initial fluid composition in the real system is not known and therefore been generated by using a “neutral” fluid, which evolves during time until the system reaches steady-state conditions. The final fluid composition from that simulation is then used for further modeling.

Initial fluid composition for simulation 3 (inmod02):

- Ctot.H⁺ 1.000e-7
- Ctot.Na⁺ 1.000e-8
- Ctot.Cl⁻ 5.000e-8
- Ctot.Ca⁺⁺ 1.000e-8
- Ctot.Mg⁺⁺ 1.000e-8
- Ctot.K⁺ 1.000e-10
- Ctot.SiO₂_aq 1.000e-1
- Ctot.Al⁺⁺⁺ 1.000e-12

Initial fluid composition for simulation 4 and 8 (inmod04, inmod08):

- Ctot.H⁺ 1.2104e-09
- Ctot.Na⁺ 3.2163e-04
- Ctot.Cl⁻ 4.1005e-09
- Ctot.Ca⁺⁺ 1.7125e-09
- Ctot.Mg⁺⁺ 7.6940e-09
- Ctot.K⁺ 2.2486e-06
- Ctot.SiO₂_aq 6.6722e-04
- Ctot.Al⁺⁺⁺ 1.0243e-12

Initial fluid composition for simulation 5 (inmod05):

- Ctot.H⁺ 1.2418e-09
- Ctot.Na⁺ 3.3030e-04
- Ctot.Cl⁻ 5.5881e-09
- Ctot.Ca⁺⁺ 2.9845e-09
- Ctot.Mg⁺⁺ 8.0624e-09
- Ctot.K⁺ 2.3069e-06
- Ctot.SiO₂_aq 6.6725e-04
- Ctot.Al⁺⁺⁺ 1.0509e-12

Initial fluid composition for simulation 7 and 8 (test13, test14):

- Ctot.H⁺ 1.2418e-09
- Ctot.Na⁺ 3.3030e-04
- Ctot.Cl⁻ 5.5881e-09
- Ctot.Ca⁺⁺ 2.9845e-09
- Ctot.Mg⁺⁺ 8.0624e-09
- Ctot.K⁺ 2.3069e-06

- Ctot.SiO₂_aq 6.6725e-04
- Ctot.Al⁺⁺⁺ 1.0509e-12

Results

The following simulations were undertaken in order to see the dependency of grain dissolution and precipitation on temperature and compare the modelled results with the observed data. Note that all simulations are exclusively geochemical models and do not simulate rock pressure or physical changes due to compaction and overburden. Pressure changes are restricted to fluid pressure. The mineral composition had to be simplified because of complications with the NUFT code. Therefore, albite, K-feldspar, quartz, phlogopite (biotite) and montmorillonite (as a substitute for illite) have been used. All minerals that contain iron were removed because reaction progress is highly sensitive to variation in oxygen partial pressure. Such sensitivity increases the time required to complete a simulation by orders of magnitude, thus restricting the ability to examine the response of the system to variations in initial conditions. For that reason, it was decided to restrict simulations to non-Fe systems. As previously stated the code models chemical reactions. Although a wide variety of clays and chlorites can be included in the simulations, the quality of thermodynamic data for them varies widely. For that reason, it was decided to use a clay mineral for which the thermodynamic data are best known. The highest heating temperature is limited to 300°C, which is the temperature and pressure range used in the table of thermodynamic properties for aqueous speciation by the code. Sills have temperatures of ~1100°C during intrusion. However, vitrinite reflectance data from the Skye sample set (Schmid, 2006) indicate a maximum heating of the sandstone in direct contact to the sill of ~250-270°C. Relative proportions of mineral dissolution and precipitation should be representative, while total amount might be lower compared to real sill emplacement.

Case (1) Sandstone (quartzite) with porosity of 40% and temperature of 30°C

The modeling of an unconsolidated quartzite with a porosity of 40% under a temperature of 30°C shows that no mineral dissolution occurs and no porosity loss or temperature changes take place within a modelled time of 100 years, 1000 years and 100.000 years. The initial aqueous pore phase was simulated to represent marine waters.

Case (2) Sandstone (quartzite) with porosity of 25% and temperature of 90°C

The parameters of the modeling of quartzite are: porosity of 25% under a temperature of 90°C and an initial aqueous pore phase composition of marine water and saturated with 600ppm SiO₂. The silica was introduced in the fluid by dissolution of feldspars. The first simulation was without the SiO₂ aqueous component and the result showed no quartz precipitation or dissolution. In the second simulation silica was added to the aqueous phase, forcing a supersaturated fluid condition. All quartz that precipitated (0.053%) from the aqueous phase happened within the first time step of 1 year. All oversaturated silica precipitated in the first time step and the aqueous phase reached equilibrium quickly.

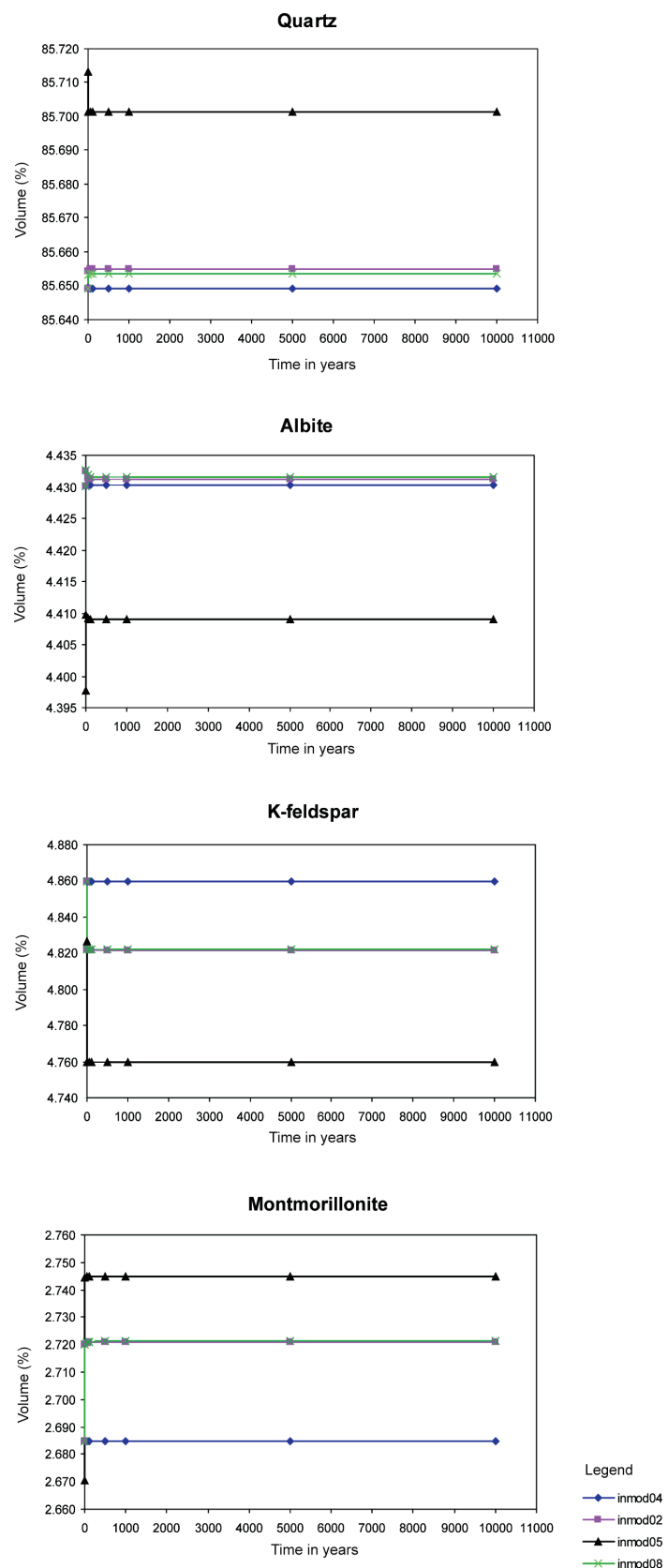


Figure 2. Temporal changes in mineral abundance for four different simulations (note there are minimal changes in the first time step and non afterwards). All mineral abundance has been normalised to 100% (porosity was removed).

Case (3) Sandstone (sample 110) with porosity of 25%, temperature of 90°C, neutral fluid and fluid flow activated, simulated time 10.000 years (inmod02)

Fluids evolve during burial over time mostly from dissolution of minerals such as feldspars. Since the initial fluid composition of the system is unknown it has to be modelled until the fluid is in a steady-state condition with the enclosing rock matrix, i.e., fluid-rock interaction is minimal and close to equilibrium. In test 3 we simulated this process over 10.000 years. This simulation shows that steady-state conditions were established soon after initiating flow. During the simulation albite, K-feldspar, phlogopite and quartz dissolved, while montmorillonite precipitated (Fig. 2).

Case (4) Sandstone (sample 110) with porosity of 25%, temperature of 90°C, fluid from simulation 3 and fluid flow activated, simulated time 10.000 years (inmod04)

The simulation was carried out for the purpose to see how minerals behave in a saturated fluid. The fluid composition from simulation 3 was used in Case 4 as the initial fluid composition, and the simulation carried out for 10.000 years. This test was also required in order to prove that fluid and rock are in steady-state. All minerals in Case 4 – albite, K-feldspar, quartz, montmorillonite and phlogopite - did not change volume during the modeling process (Fig. 2).

Case (5) Sandstone (sample 110) with porosity of 18%, temperature of 120°C, and initial fluid from simulation 4 and fluid flow activated, simulated time 10.000 years (inmod05)

In simulation 5 we tried to see if steady-state fluid will change if porosity is smaller and temperature higher. The porosity of 18% and 120°C should reflect deeper buried sandstone that theoretically has higher mineral dissolution rates. The result shows that albite dissolved slightly over 10.000 years, K-feldspar and phlogopite dissolved relatively large amount immediately after introducing the fluid, montmorillonite precipitated and quartz was dissolved immediately after introducing the fluid but later re-precipitated slightly. Porosity increased from 18 to 18.2%. The results indicate that the fluid-rock system was not close to equilibrium and the first reactions occurred as a result of establishing new steady-state conditions for the increased temperature (Fig. 2).

Case (6) Sandstone (sample 110) with porosity of 25%, temperature of 90°C, fluid from simulation 3 and fluid flow deactivated, simulated time 10.000 years (inmod08)

Geological systems that trigger diagenetic reactions can be open and closed in terms of fluid flow. It means that depending on scale and properties fluids could escape and leave not enough time for authigenic mineral precipitation. On the contrary, in closed systems fluid flow is minimal or absent and authigenic minerals are a result of dissolution of neighbouring detrital grains. The simulation results show albite, K-feldspar, phlogopite and quartz dissolving shortly after initiating the system and montmorillonite precipitating. All changes occur in the first time step, which indicates that the system reacts to the fluid and adjusts immediately. No mineral reactions occur afterwards. It is to note that a non-fluid flow is highly unlikely since sill emplacement and property changes such as temperature and pressure might trigger fluid flow or local circulation. Therefore, a system with an active fluid flow is used for further simulations (Fig. 2).

Case (7) Sandstone (sample 110) with porosity of 25%, starting temperature of 90°C, heating up to 300°C, heated cells 9 out of 36 (cells 1-9), simulated time 10.000 years (test13)

In simulation 7 heating and cooling have been added to specific cells. For simplicity mineral composition and porosity stayed equal for heated and unheated cells. That scenario should test what impact heating and cooling has on mineral and fluid reactions without chemical or physical differences. The sandstone is the same as before – slightly modified sample 110 – subfeldspathic arenite with a porosity of 25% as measured in sample 110. Heating and

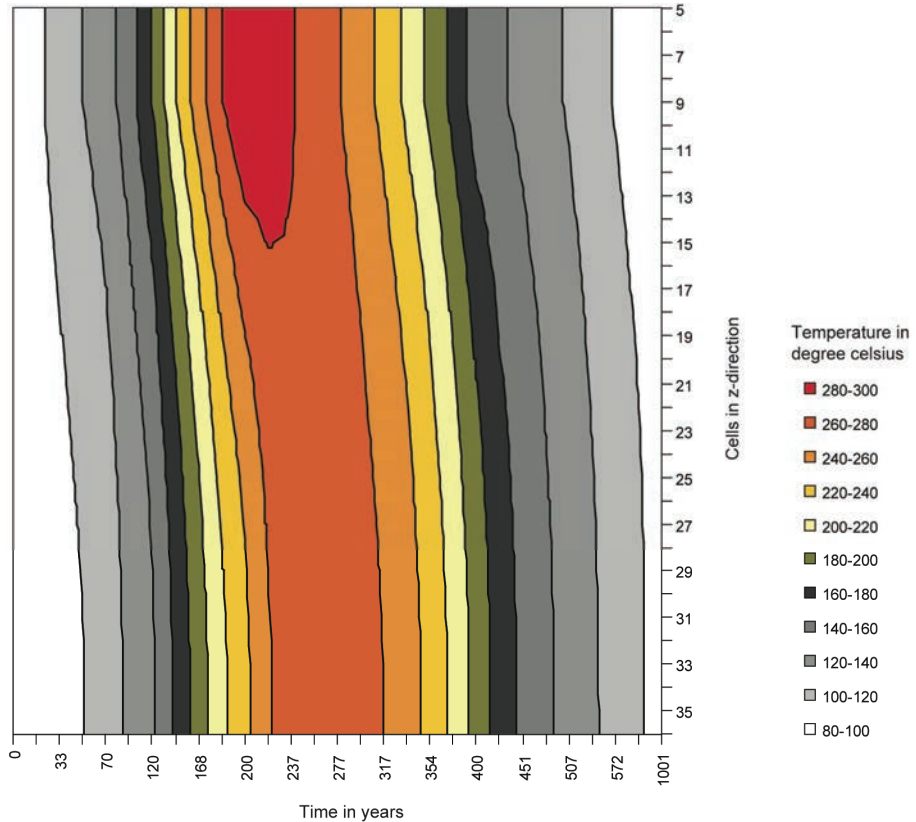


Figure 3. Temporal changes of temperature (simulation 7) with distance to heated source (cells 5 to 9). Plot represents the fluid heating and cooling along the flow path (downwards).

cooling took place slightly longer to estimated real time processes. The reason is that a very rapid temperature increase can only be modelled if very small time steps are taken because the mathematical problem is very hard to solve. By stretching out the heating time the problem is easier to solve. Background temperature is 90°C and controlled temperature stages are: 0 years - 90°C, 10 years - 95°C, 50 years - 120°C, 100 years - 150°C, 200 years - 300°C, 300 years - 250°C, 400 years - 150°C, 600 years - 90°C and 10.000 years - 90°C. The temperature (Fig. 3) behaviour is very reasonable, since the simulation imposed a high cooling rate that propagates through the rock. So once cooling starts, the cells downstream will lag behind. The highest temperatures in the non-heated part (cell 10 to 15) almost reach the temperature of the heated cells. The relative proportion of the number of heated cells (comparable to thickness) to the number of surrounded cells that have been intensely heated is 9 to 5 or almost 2:1. However, fluids in all sandstone cells have been heated above 260°C during the top heating temperature of 300°C.

Mineral abundance changes are recorded as follows:

Albite (Fig. 4) dissolved immediately after heating started. It started to precipitate on the contact between the heated cells and the adjacent cell above 160°C and reached maxi-

mum precipitation with the highest temperature of 300°C. Precipitation turned into dissolution along the contact during cooling and stayed elevated up to 100°C cooling temperature. Cells further away from the contact exhibited minor dissolution throughout the temperature changes. One notable example of dissolution occurred in the second cell below the contact during temperatures of 219°C to 300°C (cells itself have a temperature between 214 and 289°C). The volume in the heated cells increased from 3.300% to 3.307% and decreased in the sandstone from 3.300% to 3.297%.

K-feldspar (Fig. 5) dissolved throughout all cells except along the contact. The contact shows precipitation directly at the contact and parallel dissolution just below from a temperature between 180 and 300°C (177 to 295°C in the cell below). With cooling the reversed process takes place and the precipitated K-feldspar dissolves while new K-feldspar precipitates. The contact reaches opposite results with dissolved K-feldspar along the contact and precipitated K-feldspar just below with cooling temperatures of 160°C (163°C for the cell below). The volume in the heated cells varies from 3.616% to 3.628% (3.620% initially) and in the sandstone varies from 3.613% to 3.624% (3.620% initially).

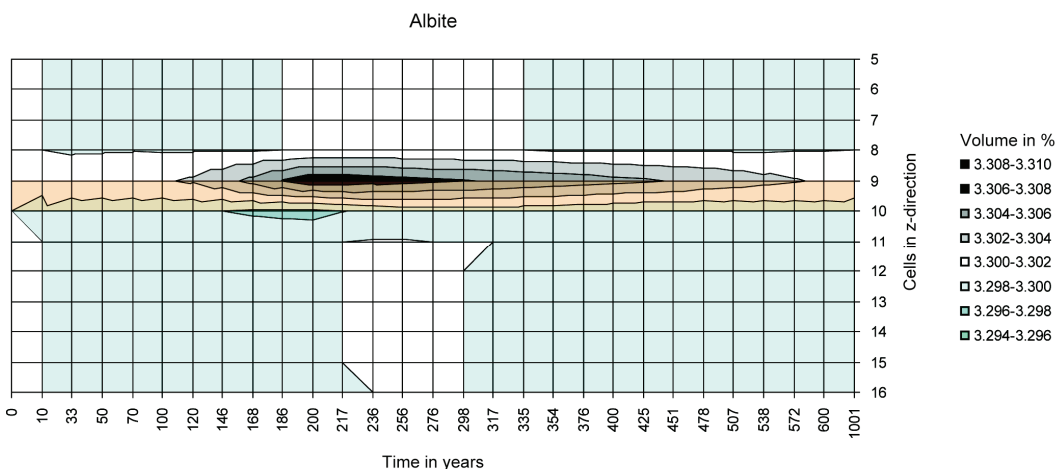


Figure 4. Temporal changes of albite content (simulation 7) during heating and cooling. Contact zone is highlighted orange. White colour represents initial albite volume, shades of grey represent increased albite abundance and greenish colours represent albite dissolution.

Montmorillonite (Fig. 6) was stable in all cells distal to the contact. Significant dissolution along the contact started with a temperature of 150°C and peaked at 300°C. Parallel precipitation took place below the contact along the fluid path starting with a temperature of 148°C up to 295°C. A reverse reaction of dissolution and precipitation took place during cooling below 100°C. The volume in the sill varies from 1.987% to 2.023% (2.000% initially) in the sandstone varies from 1.998% to 2.009% (2.000% initially).

Quartz (Fig. 7) dissolved slightly throughout the simulation. Precipitation occurred along the contact from a temperature of 219°C to 300°C and dissolved afterwards. Quartz in the cell below the contact dissolved parallel to the precipitation equally and precipitated afterwards. A reverse trend occurred with cooling temperatures below 196°C. The volume in the heated cells varies from 63.76% to 63.90% (63.80% initially) and in the sandstone varies from 63.71% to 63.85% (63.80% initially).

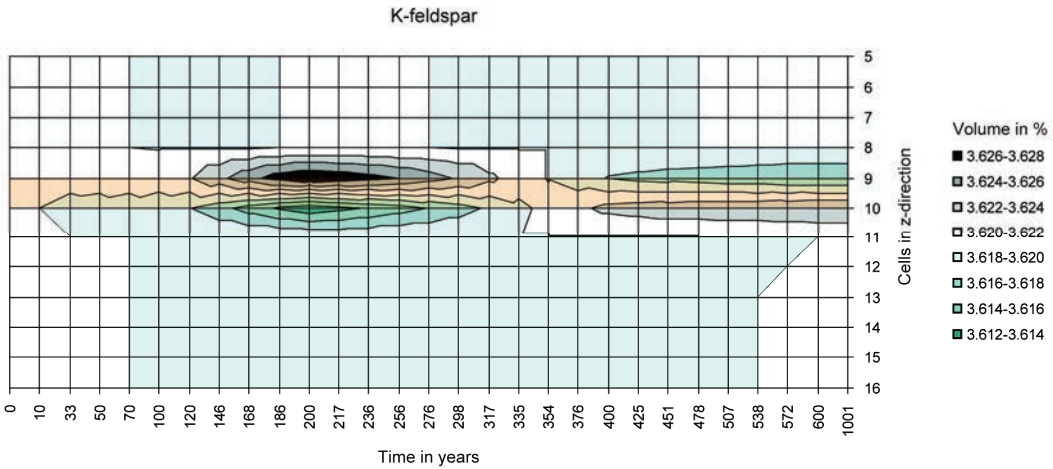


Figure 5. Temporal changes of K-feldspar content (simulation 7) during heating and cooling. Contact zone is highlighted orange. White colour represents initial K-feldspar volume, shades of grey represent increased K-feldspar abundance and greenish colours represent K-feldspar dissolution.

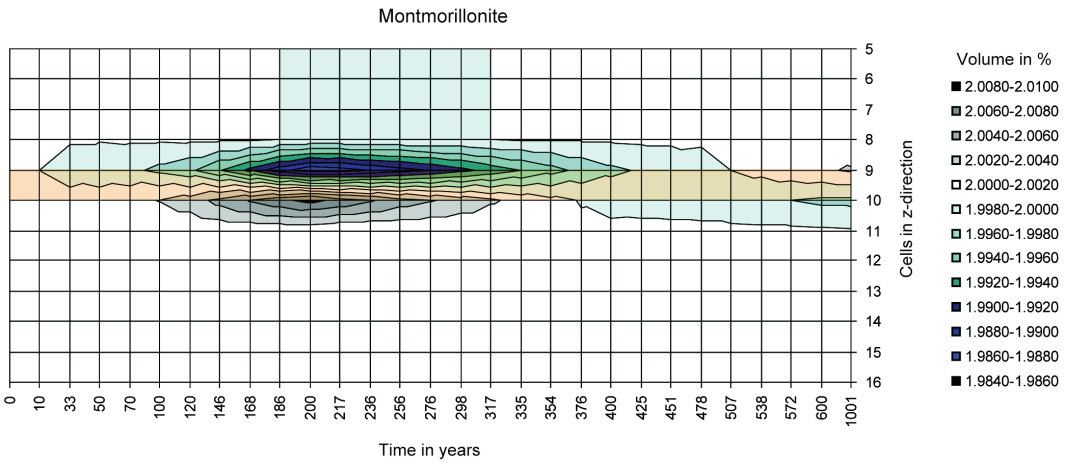


Figure 6. Temporal changes of montmorillonite content (simulation 7) during heating and cooling. Contact zone is highlighted orange. White colour represents initial montmorillonite volume, shades of grey represent increased montmorillonite abundance and greenish colours represent montmorillonite dissolution.

Porosity (Fig. 8) reflects the main mineral precipitation and dissolution trends spatially and in time. It did not change except along the contact or immediately below. At the contact porosity decreased, while the cell below had an increase in porosity. The porosity in the heated cells ranges from 24.901% to 25.042% (25.000% initially) and in the sandstone ranges from 24.952% to 25.094% (25.000% initially). The trend reversed sharply with a cooling temperature of 233°C.

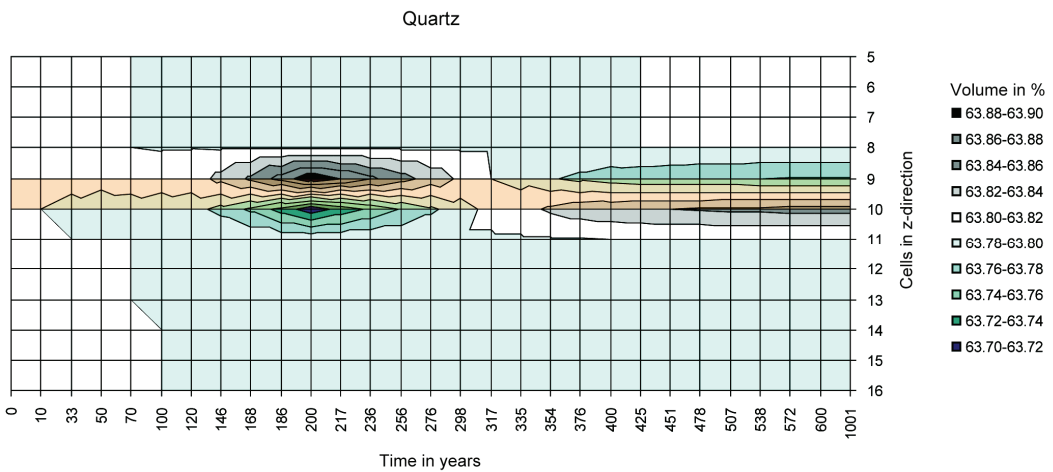


Figure 7. Temporal changes of quartz content (simulation 7) during heating and cooling. Contact zone is highlighted orange. White colour represents initial quartz volume, shades of grey represent increased quartz abundance and greenish colours represent quartz dissolution.

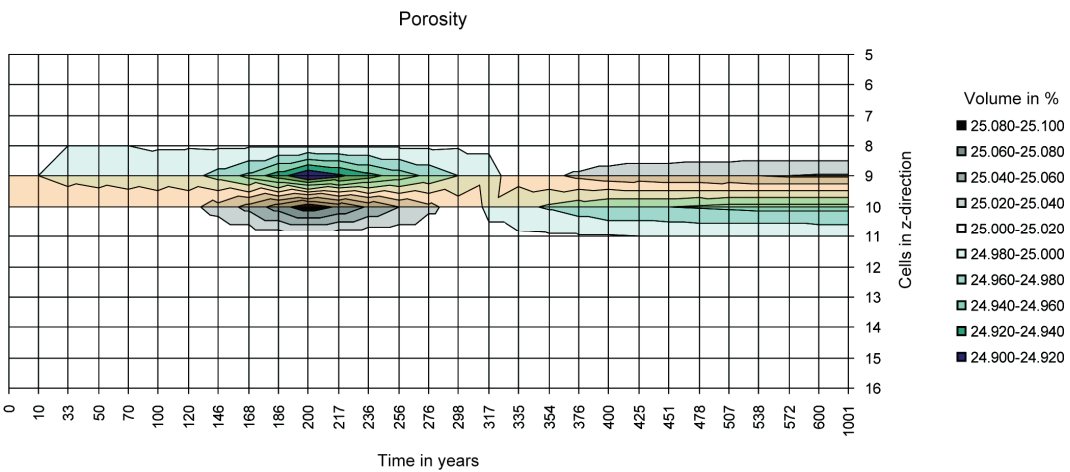


Figure 8. Temporal changes of porosity (simulation 7) during heating and cooling. Contact zone is highlighted orange. White colour represents initial porosity, shades of grey represent increased porosity and greenish colours represent porosity loss.

Case (8) Sandstone (sample 110) with porosity of 10% (cell 4-8) and 25% (cells 9-36) and sill (basalt CIPW-norm sample 101) with porosity of 3%, starting temperature of 90°C, heating up to 250°C, heated cells 1-3 out of 36, simulated time 10.000 years (test14)

In simulation 8 heating and cooling have been added to specific cells in order to model sill that is emplaced in sandstones, and porosity has been adjusted to real data. That scenario should test what impact heating and cooling has on mineral and fluid reactions with chemical or physical differences. The sandstone is the same as before – slightly modified sample 110 – subfeldspathic arenite. The porosity remained 25% for cells 9 to 36 and set to 10% for cells 4 to 8. The Skye and Traill Ø data show porosities of ~10% close to sill contacts. Cells 1 to 3 have been adjusted to a mineral composition close to sills or in that case basalt. The porosity was set to 3%. Heating and cooling took place slightly longer to approach

real time processes. The reason is that a very rapid temperature increase can only be modelled if very small time steps are taken because the mathematical problem is very hard to solve. Background temperature is 90°C and controlled temperature stages are: 0 years - 90°C, 10 years - 95°C, 50 years - 120°C, 100 years - 150°C, 200 years - 250°C, 300 years - 150°C, 400 years - 120°C, 600 years - 90°C, 1000 years - 90°C and 10.000 years - 90°C. The temperature (Fig. 9) behaviour is very reasonable, since the simulation imposed a high cooling rate that propagates through the rock. So once cooling starts, the cells downstream will lag behind. The highest temperatures in the non-heated part (cell 4 to 6) almost reach the temperature of the heated cells. The relative proportion of the number of heated cells (comparable to thickness) to the number of surrounded cells that have been intensely heated is 4 to 2 or 2:1. However, fluids in all sandstone cells have been heated above 190°C during the highest heating temperature of 250°C.

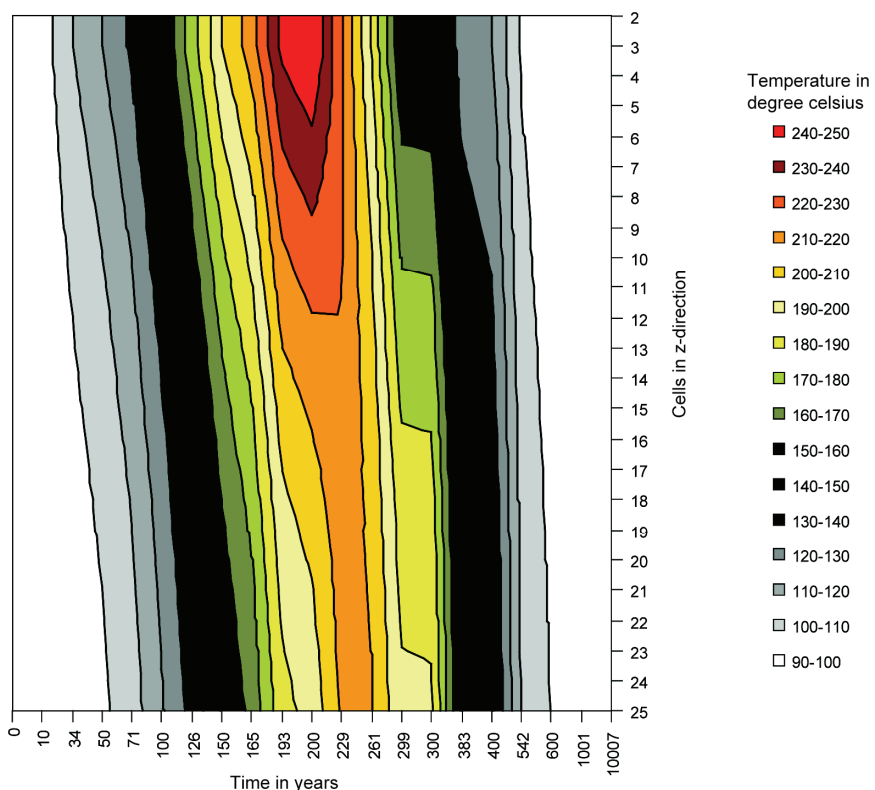


Figure 9. Temporal changes of temperature (simulation 8) with distance to heated source (cells 2 to 3). Plot represents the fluid heating and cooling along the flow path (downwards).

Mineral abundance changes are recorded as follows:

Albite (Fig. 10) dissolved immediately after heating started. It started to precipitate on the contact between the heated cells and the adjacent cell during the cooling at around 222°C and reached maximum precipitation around 200°C. Precipitation turned into slow dissolution along the contact during cooling but the albite volume stayed above original volume during 10.000 years simulating time. Cells further away from the contact exhibited minor dissolution throughout the temperature changes. There is no notable change between the different sandstone porosities. Albite content of the sill in the contact decreased slightly.

Albite content in the sandstone along the contact decreased with heating up to 246°C and increased abruptly with onset of cooling, reaching a maximum at ~200°C. The volume in the sill decreased to 27.325% (27.330% initially) and in the sandstone varies from 3.947% to 3.959% (3.950% initially).

K-feldspar (Fig. 11) dissolved throughout all cells. The contact shows precipitation in the sill cells at the contact and parallel dissolution just below in the sandstone from a temperature between 110 and 250°C (108 to 246°C in the cell below). With cooling the sill K-feldspar content becomes constant at 221°C and remains at that elevated level throughout the 10.000 years simulation. While K-feldspar in the sandstone cell precipitated rapidly at 222°C and slightly dissolved again during continuing cooling. No differences were noticed between the different sandstone porosities. The volume in the sill increased to 3.015% (3.010% initially) and in the sandstone decreased to 4.330% (4.340% initially).

Montmorillonite (Fig. 12) precipitated relatively significantly along the contact in the sandstone cell during heating up to maximum temperature of 250°C and also slightly in all cells below. There was no montmorillonite in the sill cells. Rapid dissolution along the contact started during cooling and reached maximum at ~200°C. This short interval was followed by precipitation that started at 191°C and continued for 10.000 years. The total volume of montmorillonite did not reach the initial condition during the simulation. There was no change in volume between the different sandstone porosities. The volume in the sandstone varies from 2.386% to 2.402% (2.390% initially).

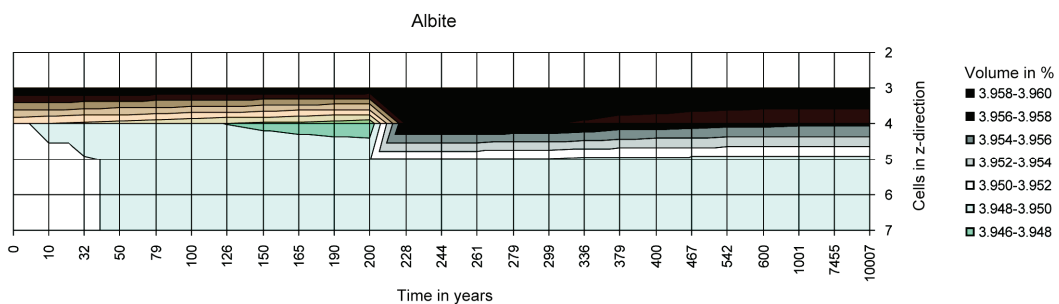


Figure 10. Temporal changes of albite content (simulation 8) during heating and cooling. Contact zone is highlighted orange. White colour represents initial albite volume, shades of grey represent increased albite abundance and greenish colours represent albite dissolution.

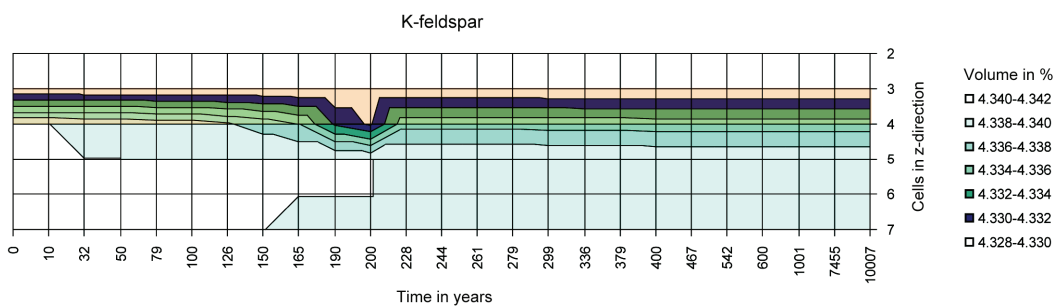


Figure 11. Temporal changes of K-feldspar content (simulation 8) during heating and cooling. Contact zone is highlighted orange. White colour represents initial K-feldspar volume, shades of grey represent increased K-feldspar abundance and greenish colours represent K-feldspar dissolution.

Quartz (Fig. 13) in the sill cells precipitated during the heating and dissolved during the cooling. Rapid precipitation in sandstones occurred with the onset of cooling after dissolution and continued throughout the simulated time of 10.000 years. It is to note that the same dissolution and precipitation trend, but with a lower magnitude took place in all cells. There was no difference in volume between the 10% and 25% porosity sandstones. The volume in the sill varies from 1.411% to 1.570% (1.470% initially, Table 14) and in the sandstone varies from 76.88% to 77.03% (76.97% initially).

Porosity (Fig. 14) in the sill contact cell decreases during heating with the maximum temperature of 250°C and increases with the onset of cooling during the complete simulation

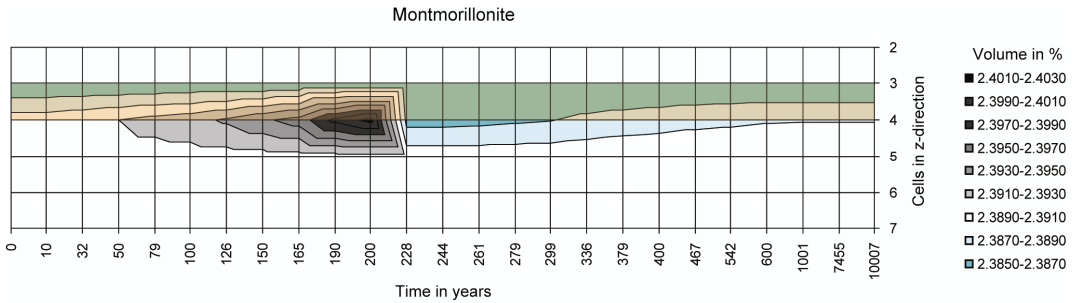


Figure 12. Temporal changes of montmorillonite content (simulation 8) during heating and cooling. Contact zone is highlighted orange. White colour represents initial montmorillonite volume, shades of grey represent increased montmorillonite abundance and greenish colours represent montmorillonite dissolution.

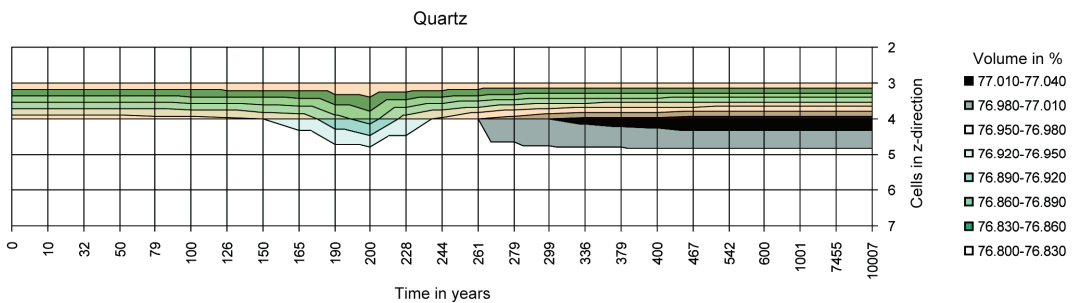


Figure 13. Temporal changes of quartz content (simulation 8) during heating and cooling. Contact zone is highlighted orange. White colour represents initial quartz volume, shades of grey represent increased quartz abundance and greenish colours represent quartz dissolution.

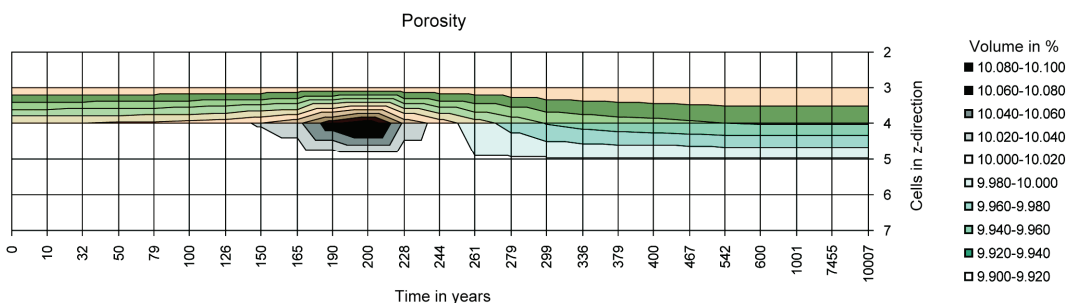


Figure 14. Temporal changes of porosity (simulation 8) during heating and cooling. Contact zone is highlighted orange. White colour represents initial porosity, shades of grey represent increased porosity and greenish colours represent porosity loss.

time. Porosity of the sandstone contact cell increases with heating and drops with onset of cooling. After 10.000 years the porosity remains below the original porosity in the 10% sandstone. Porosity in the remaining sandstone cells is either equal to the original porosity or minimal increased. The porosity in the sill ranges from 2.900% to 3.059% (3.000% initially), in the 10% porosity sandstone ranges from 9.938% to 10.098% and in the 25% porosity sandstone ranges increased to 25.002%.

The amount of dissolved potassium (Fig. 15) reached the highest values only along the contact during maximum heating and dropped back to original values with the onset of cooling. Aluminium (Fig. 16) is elevated along the contact with the onset of cooling and slowly dilutes during the 10.000 years simulation but stays above initial values. Aqueous SiO_2 (Fig. 17) increased with raising temperature and decreased during cooling throughout all cells.

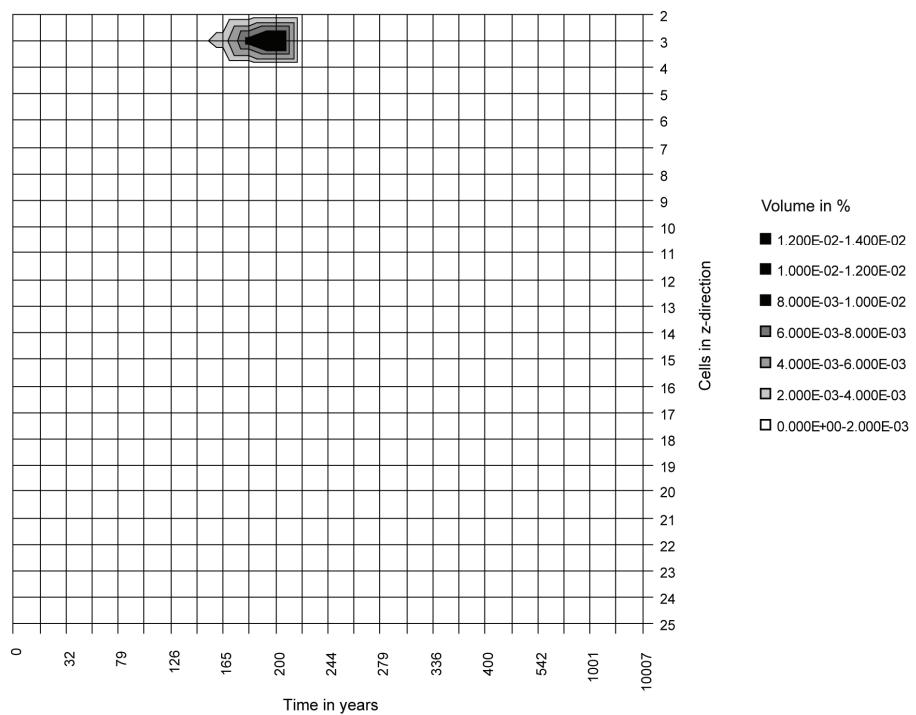


Figure 15. Temporal changes of potassium in the fluid (simulation 7) during heating and cooling. White colour represents initial potassium concentration and shades of grey represent increased potassium abundance.

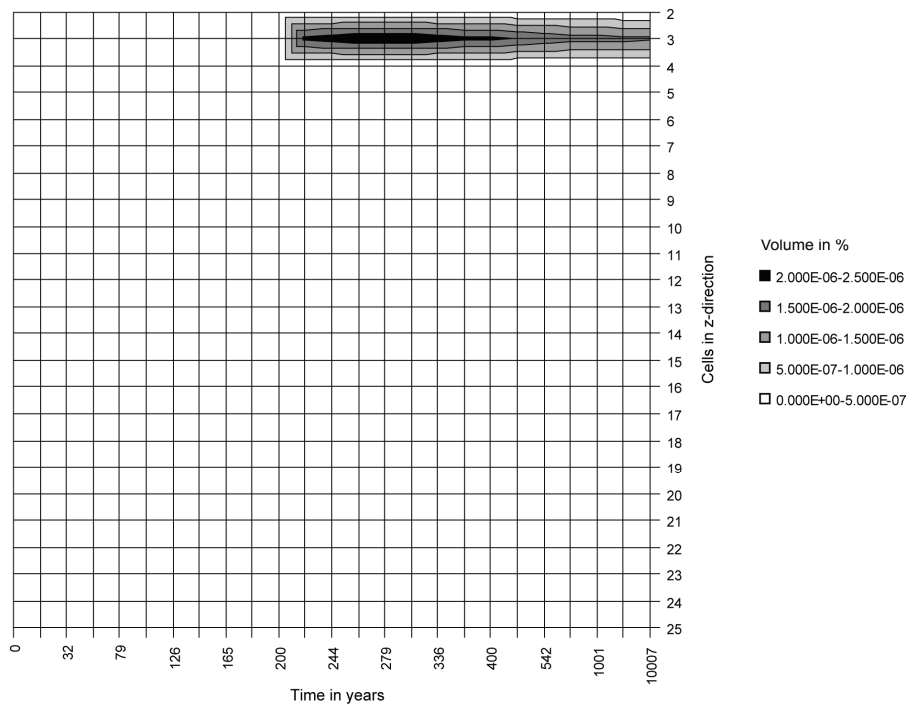


Figure 16. Temporal changes of aluminium in the fluid (simulation 7) during heating and cooling. White colour represents initial aluminium concentration and shades of grey represent increased aluminium abundance.

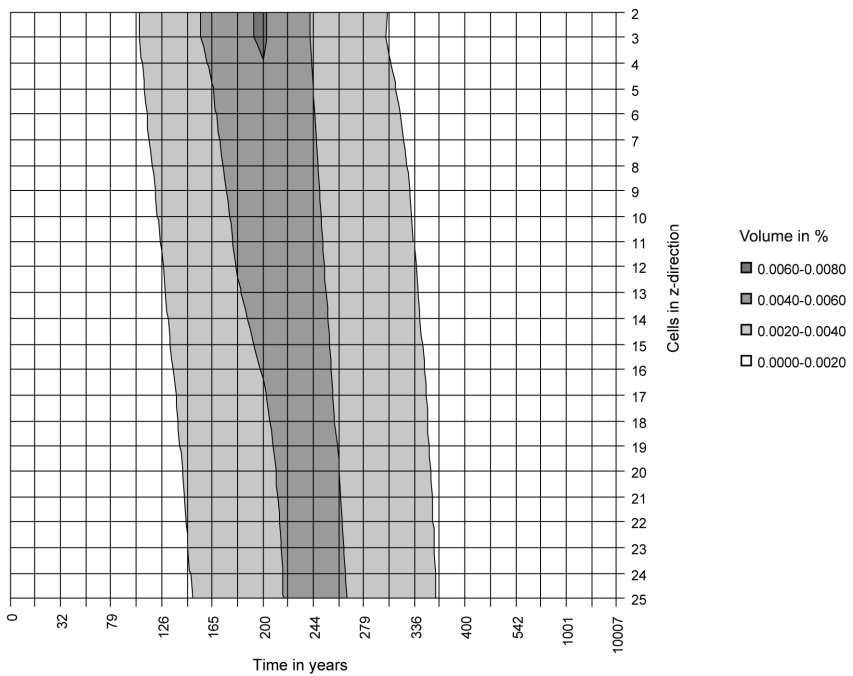


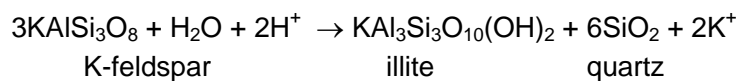
Figure 17. Temporal changes of SiO₂ in the fluid (simulation 7) during heating and cooling. White colour represents initial SiO₂ concentration and shades of grey represent increased SiO₂ abundance.

Interpretation

The interpretation will focus on case 8 because it is closest to the analogue study on Skye, Scotland. The processes that took place were also found in other simulations carried out during this study.

Heating processes

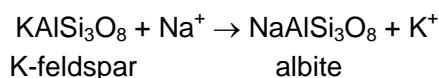
The heating phase of the sandstone initiated clay precipitation, quartz dissolution, albite dissolution and K-feldspar dissolution. Clay precipitation – in this case montmorillonite as a substitute for illite or illite/smectite and eventually chlorite and/or kaolinite - started with heating and occurred throughout the heating process. The amount of clay precipitated increased with the onset of K-feldspar dissolution at 130°C. The process of replacement of K-feldspar by clay – particularly illite is also described as illitisation of K-feldspar.



Quartz dissolution is dependent on temperature, which means that with increasing temperature more quartz gets dissolved until equilibrium is reached. Since, quartz solubility is proportional to temperature increase, supersaturation might not be achieved.

Cooling processes

The onset of cooling triggered a reverse reaction of the previous illitisation process. Clay dissolves, immediately releasing potassium, and K-feldspar precipitates and takes up the free potassium until the temperature drops to 222°C. Further cooling reverses the process again and illitisation of K-feldspar occurs throughout the whole simulation with a net loss of K-feldspar and montmorillonite after 10.000 years and remaining aluminium in the fluid. Albite precipitates from 222°C until a cooling temperature of 140°C. Albite can form during the process of albitisation, which is the dissolution of clastic K-feldspar.



Albitisation requires a mechanism for the removal of potassium and the supply of sodium. Sodium is in the fluid from the albite dissolved during heating, while potassium is precipitated with clay minerals (montmorillonite). Albite has a net gain after 10.000 years.

Quartz is precipitating during the cooling phase, because the decrease in temperature hence supersaturation of quartz and subsequent precipitation. Total amount of quartz increased after 10.000 years, which is likely to be a result of the illitisation of K-feldspar that forms quartz as a product.

Porosity changes

The overall porosity decreases after 10.000 years, which is interpreted to be an effect of increased total quartz content. The decreased porosity only occurs in direct contact to the sill. The sill has not affected sandstones further away from the contact. The porosity loss described here is solely the loss from geochemical reactions and not from compaction.

Mineral abundance changes

The simulated processes are geochemically consistent with processes that have been experimentally studied or observed. Illitisation, albitisation and quartz precipitation are common features during burial diagenesis and usually take place over several million years and are dependent on temperature and pressure. Sill emplacement and the relatively fast temperature changes force these processes to happen in a short time interval. The amount of e.g. authigenic quartz found in sandstones that experienced more than 150°C and a depth of ~4000 m is commonly above 5%. The amount produced by heating during sill emplacement is 0.06%. This small number indicates that geologically rapid temperature changes and a lack of overburden in porous sediments have a minimal effect on total volume changes and subsequently on porosity.

The modeling suggests that the zone that is affected by geochemical changes during the sill emplacement is half the width of the intrusion if the host sediment is homogeneous and mineral volume and porosity changes are below 1%.

Comparison with Skye data

The Skye sandstones have been described in detail in the report on sill emplacement (Schmid, 2006). The detrital mineralogy of the sandstones is dominated by detrital quartz with a very small amount of feldspar, rock fragments and detrital clay. The most abundant authigenic phases are calcite (including ferroan calcite) and quartz overgrowth, which make up to 31.50-40.75% and 1-8.67% of the rock volume respectively. Other diagenetic phases present in small amounts include pyrite, kaolin, chlorite and illite. The sandstones have experienced diagenetic alteration involving mechanical and chemical compaction, mineral precipitation and feldspar grain dissolution.

The sandstones in the studied samples are well compacted with textural evidence for both mechanical and chemical compaction present. Detrital muscovite grains commonly are bent and distorted around quartz grains. Concavo-convex, linear and sutured contacts between quartz grains provide evidence for intergranular pressure solution and compaction. The process of compaction clearly degraded the porosity-permeability properties.

Porosity-depth trends (e.g. Ramm, 1992; Ramm & Bjørlykke, 1994) suggest that mechanical compaction occurs in a linear manner until a temperature threshold which chemical compaction dominates (~90°C in Jurassic sandstones of the North Sea). Early cementation can also retard mechanical compaction (Fisher et al., 1999).

Chemical compaction (pressure solution) refers to the process of mineral dissolution at stressed grain-contacts. In quartzose sandstones, the time-temperature history is probably the most important variable affecting the diffusive mass transfer (DMT) processes involved, quartz dissolution being very slow at temperatures below 90°C but significantly at higher temperatures.

The most abundant component in the sandstones is quartz and concomitantly quartz overgrowth as the dominating authigenic phase. Detrital quartz versus distance from sill and authigenic quartz versus distance from sill show that quartz overgrowth directly correlates to the amount of detrital quartz present. There is no clear trend that the volume of quartz overgrowth is related to the distance from sill. However, detrital quartz versus authigenic quartz shows a very good correlation ($R^2 = 0.7$) implicating that the amount of quartz overgrowth is partly controlled by the total volume of quartz available during diagenesis.

The porosity ranges from 1.4 to 23.87% of the rock volume, where the lowest porosity occurs in the (pre-compaction) calcite cemented sandstones. The average porosity in sample set 2 is 8.6%, while porosities in sample set 1 vary widely (10.4% near contact and 23.9% furthest away).

The lacking correlation between cements and porosity might indicate that compaction was the responsible factor in porosity reduction rather than cementation.

The extent of the contact aureole can not be accurately predicted because sample set 1 showed less contact influence in a sample 7 m away from the contact (27% porosity corresponding to a burial depth of ~1400 m without the effect of heating from intrusions and only minor quartz cementation (1.67%)); while a sample 9.7 m away from the contact in set 2 shows clear contact influences. The sill emplacement did not affect sandstones more than 25 m away from the contact.

The Skye samples show two main observations. (1) quartz cementation correlates to total amount of detrital quartz and shows no correlation with distance from sill, and (2) the extent of the contact aureole varies between two sample sets that are a few kilometres apart.

The geochemical modeling reveals new insights into the SiO₂ system. As stated before, quartz dissolution is increasing with increasing temperature, releasing SiO₂ into the fluid, which is transported away from the contact. However, the fluid remains undersaturated with SiO₂ and no precipitation occurs. Cooling reverses the process and SiO₂ starts to precipitate along the contact but not in the amounts expected from observations made on analogue studies. In principal, silica volume is dependent on temperature, but does not precipitate. Connectivity between pores (e.g. permeability) can cause stagnating fluid flux and therefore hence quartz precipitation. The fluid flow decreases and individual pores get supersaturated with SiO₂, leading to quartz precipitation. The Skye samples with high quartz cement volume (~8%) have very low permeability, while the highly permeable sample (sample 110) has weak quartz cementation (1.67%). Additionally, rock pressure and fluid pressure increased, while permeability and porosity decreased with sill emplacement due to compaction. The changes in the rock pressure changed significantly with the intrusion and triggered grain-to-grain dissolution (pressure dissolution) and subsequent quartz cementation that cannot be modelled geochemically. The extent of SiO₂ transport with the heated fluid depends on the physical properties of the rock. In Skye set 1, a highly calcite cemented layer that has no porosity, acted as a barrier for fluid and heat transport, preventing any alteration below and limited the extent of the contact aureole to 10 cm. The low amount of quartz overgrowth in sample 102 in set 1 has yet another reason. It is currently evident that Fe-chlorite inhibits quartz cementation in deep reservoirs (pers. Comm R.H. Worden). Since there is ~9% chlorite in the sample, it might explain the unusual low amount of quartz cement.

In summary, heating of sandstones up to temperatures of 300°C does affect the sandstone porosity or authigenic mineralogy. Aqueous SiO₂ remains in the fluid, if fluid transport rate and connectivity are high. The amount of SiO₂ dissolution is directly related to temperature. The observed field data from Skye and the geochemically modelled data, although exhibiting some qualitative similarities, exhibit significant quantitative differences because (1) temperature is not the only important factor in mineral dissolution, alteration and precipitation and (2) pressure due to mechanical and chemical compaction is highly important too and cannot be modelled with the NUFT code.

Conclusion

The studies undertaken during the SINDRI project on the impact of Palaeogene sill emplacement on reservoir lithologies in East Greenland and the Faroe-Shetland Basin shows: The effect of sill emplacement on shallow-buried sandstones varies significantly depending on (1) the detrital composition of the sandstones, (2) the temperature of the intrusion and (3) the extent to which fluid flow occurs.

The detrital composition of the sandstone has an effect on (1) the compaction curve during burial and subsequently porosity changes and (2) the feasibility of cementation (e.g. clay coating prevents quartz cementation).

The temperature of the intrusion has an effect on (1) the solubility of quartz (quartz becomes more likely to dissolve with increasing temperatures) and subsequent quartz cementation, (2) the degree of clay mineral replacement resulting in permeability loss and (3) the extent of mineral alterations (e.g. metasomatism, albitisation and chloritisation).

Permeability and porosity are highly reduced due to the intrusion in the contact aureole due to mechanical and chemical compaction and associated authigenic mineral precipitation and alteration.

The effect of fluid flow is to transport solutes, which modifies the extent of local dissolution and precipitation. Rapid fluid flow can prevent or diminish the extent of precipitation and will thus significantly impact the degree of cementation.

The geochemical modeling shows that the temperature increase in the sediment due to sill emplacement has no significant impact on porosity, for the conditions assumed in these simulations. However, mineral dissolution and reprecipitation such as illitisation and K-feldspar dissolution occur. The geochemical modeling did not reproduce quantitatively the observed diagenetic changes in sandstones from Skye. The Skye samples have major quartz cementation (~8%), while the modelled results are below 1%. This implies that the temperature is not the overall control in mineral precipitation, or that flow and surface area properties in the simulations did not accurately reproduce those in the natural system. Other variables such as pressure due to sill emplacement must play a significant role too. Neither can be modelled using the NUFT code.

Therefore, it is suggested that the definition of the contact aureole has to distinguish between **chemical** contact aureole and **physical** contact aureole. The chemical or geochemical contact aureole defines the zone of geochemical changes (dissolution and precipitation of minerals) stimulated by heating and subsequent cooling. The modeling suggests a zone which is half the width of the intrusion if the intruded sediment is homogeneous. Mineral changes or porosity changes are only minimally effected by the intrusion. The physical contact aureole defines the zone of physical changes (compaction, fracturing and grain rearrangement) caused by space generation and pressure changes during emplacement. The extent in homogeneous sediments varies with the thickness of the intrusion and overburden during emplacement.

Significant cementation and reduction of porosity and permeability can only occur in the zone where physical and chemical contact aureoles overlap because physical processes such as compaction force grain-to-grain dissolution and permeability loss that prevent geochemical processes such as fluid flow and hence precipitation due to supersaturation. The result can be a highly quartz cemented sandstone as seen on Skye.

The implications for the Faroe-Shetland Basin are that the chemical contact aureole can be mathematically estimated from the thickness of the intrusion. The physical contact aureole can also be mathematically estimated from known overburden, rock density (or sonic density, SGR) and thickness of intrusion. The cementation zone should then be in the overlapping zone of both.

The next two examples should show how overburden and initial burial depth is significant for estimating the impact of the intrusion.

1) If the intrusion is 200 m thick the chemical contact aureole should be approximately 100 m. The overburden before the intrusion is 100 m. That means that the sandstone is unconsolidated and has no significant overburden. Therefore, the physical contact aureole should be absent or restricted to a few centimetres. Unconsolidated, homogeneous sandstone has a porosity of 40 to 45% and as shown from the Greenland and Skye samples, porosity loss during sill emplacement is not more than 10%. 30% porosity sandstone has low grain-to-grain boundaries and therefore limits dissolution of minerals and also does not inhibit fluid flow.

2) The intrusion is 200 m thick and the chemical contact aureole is 100 m thick. The overburden before the intrusion is 3000 m. That means that the sandstone has an initial porosity of ~20% or less and grain rearrangement as well as pressure dissolution already started as cause of burial. Sill emplacement reduces the porosity to 10% and subsequent mineral dissolution diminishes porosity further to eventually zero porosity.

The intrusion thickness and geochemical changes or geochemical contact aureole would be the same in both cases, even with different porosities (implying good connectivity or permeability). However, pressure dissolution it is more likely to occur in lower porosity rocks, which implies that cementation impact caused by compaction during the emplacement of intrusions in initially deeper buried sandstones is more likely to be higher than in shallow buried sandstones.

Acknowledgments

The work on geochemical modeling and interpretation presented in this volume was performed during the project “Impact of Palaeogene sill emplacement on reservoir lithologies in East Greenland and the Faroe-Shetland Basin” funded by the SINDRI group. The SINDRI group was established by the Minister of Petroleum for the Faroe Islands (August 2001). It was formed as a result of the requirement for licensees within the Faroese area to fund and carry out projects of relevance to the future investigation of the Faroese continental shelf.

The current licensees are:

Agip Denmark BV
Amerada Hess (Faroes) Ltd.
Anadarko Faroes Company
P/F Atlantic Petroleum
BP Amoco Exploration Faroes Ltd.
British Gas International BV
DONG Føroyar P/F
Enterprise Oil Exploration Ltd.
Føroya Kolvætni P/F
Petro-Canada Faroes GmbH
Phillips Petroleum Europe Exploration Ltd.
Shell (UK) Ltd.
Statoil Færøyene AS

The intensive help of William Glassley getting the NUFT code working and finding solutions for many difficulties is highly acknowledged.

References

- Fisher, Q.J., Casey, M., Chennell, M.B. & Knipe, R.J. 1999. Mechanical compaction of deeply buried sandstones. *Marine and Petroleum Geology* 16, 605-618.
- Glassley, W.E., Nitao, J.J., Grant, C.W., Boulos, T.N., Gokoffski, M.O., Johnson, J.W., Kercher, J.R., Levatin, J.A. & Steefel, C.I. 2001. Performance Prediction for Large-Scale Nuclear Waste Repositories: Final Report. Lawrence Livermore National Laboratory, UCRL-ID-142866, 41p.
- Kühn, M. 2004. Reactive Flow Modeling of Hydrothermal Systems. Springer Verlag, 261p.
- Konikow, L.F. & Bredehoeft, J.D. 1992. Groundwater models can not be validated. *Advances in Water Resources* 15, 75-83.
- Nitao, J.J. 1998. User's Manual for the USNT Module of the NUFT Code, Version 2.0 (NP-Phase, NC-Component, Thermal). Lawrence Livermore National Laboratory, UCRL-MA-130653, 76p.
- Ramm, M. 1992. Porosity-depth trends in reservoir sandstones: offshore Norway. *Marine and Petroleum Geology* 9, 553-567.
- Ramm, M. & Bjørlykke, K. 1994. Porosity-depth trends in reservoir sandstones – assessing the quantitative effects of varying pore-pressure, temperature history and mineralogy, Norwegian Shelf data. *Clay minerals* 29, 4, 475-490.
- Schmid, S. 2006. Impact of Palaeogene sill emplacement on reservoir lithologies in East Greenland and the Faroe-Shetland Basin, Rapport 2006/54, Geological Survey of Denmark & Greenland, 80p.

Appendix

Geochemical modeling tables

run	time sec	time yrs	CtotMolal.H+	CtotMolal.Na+	CtotMolal.Cl-	CtotMolal.Ca++	CtotMolal.Mg++	CtotMolal.K+	CtotMolal.SiO2_aq	CtotMolal.Al+++
inmod04 90C,sat fluid flow	0	0	1,210E-09	3,216E-04	4,100E-09	1,712E-09	7,694E-09	2,249E-06	6,672E-04	1,024E-12
	3,16E+07	1	1,181E-09	3,589E-04	4,614E-09	1,927E-09	6,562E-09	2,204E-06	6,659E-04	1,013E-12
	1,58E+09	50	1,161E-09	3,372E-04	4,617E-09	1,929E-09	6,246E-09	2,168E-06	6,653E-04	9,967E-13
	3,16E+09	100	1,161E-09	3,370E-04	4,621E-09	1,933E-09	6,243E-09	2,168E-06	6,653E-04	9,966E-13
	1,58E+10	500	1,162E-09	3,371E-04	4,655E-09	1,968E-09	6,246E-09	2,169E-06	6,653E-04	9,968E-13
	3,16E+10	1001	1,162E-09	3,371E-04	4,698E-09	2,011E-09	6,246E-09	2,169E-06	6,653E-04	9,969E-13
	1,58E+11	5003	1,163E-09	3,372E-04	5,041E-09	2,357E-09	6,245E-09	2,171E-06	6,656E-04	9,973E-13
	3,16E+11	10007	1,163E-09	3,234E-05	5,466E-09	2,788E-09	6,245E-09	2,172E-06	6,659E-04	9,978E-13
	0	0	1,000E-07	1,000E-08	5,000E-08	1,000E-08	1,000E-08	1,000E-10	1,000E-01	1,000E-12
inmod02 90C,unsat flow	3,16E+07	1	1,314E-08	2,208E-07	5,598E-13	1,156E-13	7,738E-07	2,574E-05	6,377E-04	1,287E-11
	1,58E+09	50	1,546E-09	2,370E-04	3,120E-09	6,257E-10	1,098E-08	2,882E-06	6,653E-04	1,327E-12
	3,16E+09	100	1,188E-09	3,118E-04	3,124E-09	6,296E-10	6,520E-09	2,217E-06	6,653E-04	1,019E-12
	1,58E+10	500	1,131E-09	3,281E-04	3,158E-09	6,640E-10	5,916E-09	2,111E-06	6,653E-04	9,703E-13
	3,16E+10	1001	1,131E-09	3,281E-04	3,200E-09	7,072E-10	5,916E-09	2,111E-06	6,654E-04	9,703E-13
	1,58E+11	5003	1,132E-09	3,282E-04	3,539E-09	1,053E-09	5,915E-09	2,113E-06	6,656E-04	9,708E-13
	3,16E+11	10007	1,133E-09	3,283E-04	3,935E-09	1,479E-09	5,916E-09	2,114E-06	6,659E-04	9,713E-13
	0	0	1,242E-09	3,303E-04	5,588E-09	2,985E-09	8,062E-09	2,307E-06	6,673E-04	1,053E-12
	3,16E+07	1	2,326E-08	2,679E-07	2,499E-13	1,357E-13	2,417E-07	4,248E-05	1,162E-03	1,256E-11
inmod05 120C, sat fluid flow	1,58E+09	50	3,079E-09	3,157E-04	8,665E-10	4,643E-10	4,470E-09	5,620E-06	1,163E-03	1,661E-12
	3,16E+09	100	2,608E-09	3,761E-04	8,721E-10	4,700E-10	3,218E-09	4,762E-06	1,163E-03	1,407E-12
	1,58E+10	500	2,563E-09	3,831E-04	9,199E-10	5,179E-10	3,109E-09	4,680E-06	1,163E-03	1,383E-12
	3,16E+10	1001	2,563E-09	3,831E-04	9,791E-10	5,775E-10	3,109E-09	4,680E-06	1,163E-03	1,383E-12
	1,58E+11	5003	2,565E-09	3,832E-04	1,450E-09	1,054E-09	3,110E-09	4,683E-06	1,163E-03	1,384E-12
	3,16E+11	10007	2,567E-09	3,833E-04	2,028E-09	1,644E-09	3,110E-09	4,687E-06	1,163E-03	1,384E-12
	0	0	1,210E-09	3,216E-04	4,101E-09	1,713E-09	7,694E-09	2,249E-06	6,672E-04	1,024E-12
	3,16E+07	1	1,316E-08	2,191E-07	5,030E-249	4,133E-249	7,759E-07	2,570E-05	6,350E-04	1,294E-11
	1,58E+09	50	1,549E-09	2,366E-04	7,726E-17	3,227E-17	1,103E-08	2,889E-06	6,653E-04	1,330E-12
inmod08 90C, sat fluid no flow	3,16E+09	100	1,188E-09	3,117E-04	7,749E-17	3,237E-17	6,529E-09	2,218E-06	6,653E-04	1,020E-12
	1,58E+10	500	1,131E-09	3,282E-04	2,126E-16	8,880E-17	5,921E-09	2,112E-06	6,653E-04	9,706E-13
	3,16E+10	1001	1,131E-09	3,282E-04	3,144E-16	1,313E-16	5,921E-09	2,112E-06	6,653E-04	9,706E-13
	1,58E+11	5003	1,131E-09	3,282E-04	3,573E-16	1,492E-16	5,921E-09	2,112E-06	6,653E-04	9,706E-13
	3,16E+11	10007	1,131E-09	3,282E-04	3,573E-16	1,492E-16	5,921E-09	2,112E-06	6,653E-04	9,706E-13

Table 3. Geochemical modeling results for inmod02, 04, 05 and 08.

Table 3...continued Modeling results for inmod02, 04, 05 and 08.

Table 4. Geochemical modeling results for temperature - test 13 (blue = sill)

Depth	Time	0,0E+00 3,2E+08 1,1E+09 1,6E+09 2,2E+09 3,2E+09 3,8E+09 4,6E+09 5,3E+09 5,9E+09 6,3E+09 6,9E+09 7,5E+09 8,1E+09 8,7E+09 9,5E+09 1,0E+10 1,1E+10 1,2E+10 1,3E+10 1,4E+10 1,5E+10 1,6E+10 1,7E+10 1,8E+10 1,9E+10 3,2E+10																											
		0	10	33	50	70	100	120	146	168	186	200	218	237	257	277	300	317	335	354	376	400	425	451	478	507	538	572	600
0	90	95	110	120	132	150	180	219	251	279	300	291	282	272	261	250	233	215	196	174	150	143	135	127	118	109	99	90	90
1	90	95	110	120	132	150	180	219	251	279	300	291	282	272	261	250	233	215	196	174	150	143	135	127	118	109	99	90	90
2	90	95	110	120	132	150	180	219	251	279	300	291	282	272	261	250	233	215	196	174	150	143	135	127	118	109	99	90	90
3	90	95	110	120	132	150	180	219	251	279	300	291	282	272	261	250	233	215	196	174	150	143	135	127	118	109	99	90	90
4	90	95	110	120	132	150	180	219	251	279	300	291	282	272	261	250	233	215	196	174	150	143	135	127	118	109	99	90	90
5	90	95	110	120	132	150	180	219	251	279	300	291	282	272	261	250	233	215	196	174	150	143	135	127	118	109	99	90	90
6	90	95	110	120	132	150	180	219	251	279	300	291	282	272	261	250	233	215	196	174	150	143	135	127	118	109	99	90	90
7	90	95	110	120	132	150	180	219	251	279	300	291	282	272	261	250	233	215	196	174	150	143	135	127	118	109	99	90	90
8	90	95	110	120	132	150	180	219	251	279	300	291	282	272	261	250	233	215	196	174	150	143	135	127	118	109	99	90	90
9	90	95	110	120	132	150	180	219	251	279	300	291	282	272	261	250	233	215	196	174	150	143	135	127	118	109	99	90	90
10	90	94	108	118	130	148	177	214	246	274	295	289	281	272	262	251	236	218	199	177	153	145	136	128	119	110	100	91	90
11	90	94	107	117	129	146	173	210	242	270	290	288	281	273	263	253	238	221	202	180	156	146	138	129	120	111	101	92	90
12	90	93	106	115	127	144	170	206	238	265	286	286	280	273	264	254	240	223	204	183	159	148	139	130	121	112	102	93	90
13	90	93	105	114	125	143	167	202	234	261	281	284	280	273	265	255	242	225	207	186	162	150	140	131	122	113	103	94	90
14	90	93	104	113	124	141	164	199	230	257	277	282	279	274	266	256	243	228	209	188	165	152	142	132	123	113	103	95	90
15	90	92	103	111	122	140	162	195	226	253	273	280	279	274	267	257	245	230	212	191	167	153	143	133	124	114	104	96	90
16	90	92	102	110	121	138	159	192	222	249	269	279	278	274	267	258	247	232	214	193	170	155	144	134	125	115	105	96	90
17	90	92	101	109	120	137	157	189	219	246	266	277	278	274	268	259	248	233	216	195	172	157	145	135	126	116	106	97	90
18	90	91	100	108	119	135	155	186	216	243	263	275	277	274	268	260	249	235	218	197	174	158	146	136	126	117	107	98	90
19	90	91	99	107	117	134	153	184	213	239	259	273	277	275	269	260	251	237	220	199	176	160	147	137	127	117	107	98	90
20	90	91	98	106	116	133	151	181	210	237	256	272	276	275	270	261	252	238	221	201	178	161	148	138	128	118	108	99	90
21	90	91	98	105	115	132	149	179	208	234	254	270	275	270	262	253	240	223	203	180	162	149	139	129	119	108	100	90	
22	90	91	97	104	114	131	147	177	205	231	251	269	275	275	270	263	254	241	224	205	182	163	150	139	129	119	109	100	90
23	90	91	97	104	114	130	146	175	203	229	249	267	274	275	271	263	255	242	226	206	184	165	151	140	130	120	110	101	90
24	90	90	96	103	113	129	144	173	201	227	246	266	274	275	271	264	256	243	227	208	185	166	152	140	130	120	110	101	90
25	90	90	96	102	112	128	143	171	199	225	244	264	273	275	271	264	256	244	228	209	186	167	152	141	131	121	110	102	90
26	90	90	95	102	111	128	142	170	197	223	243	263	273	275	272	265	257	245	229	210	188	168	153	142	131	121	111	102	90
27	90	90	95	101	111	127	141	168	196	221	241	262	272	275	272	265	258	246	230	211	189	168	154	142	132	122	111	102	90
28	90	90	95	101	110	126	140	167	194	220	239	261	272	275	272	265	258	247	231	212	190	169	154	142	132	122	112	103	90
29	90	90	95	101	110	126	140	166	193	219	238	260	272	275	272	266	259	247	232	213	191	170	155	143	132	122	112	103	90
30	90	90	94	100	110	125	139	165	192	218	237	259	271	275	272	266	259	248	233	214	191	170	155	143	133	122	112	103	90
31	90	90	94	100	109	125	138	164	191	217	236	259	271	275	273	266	259	248	233	214	192	171	155	143	133	123	112	103	90
32	90	90	94	100	109	125	138	164	191	216	235	258	271	275	273	266	260	249	234	215	192	171	156	144	133	123	112	104	90
33	90	90	94	100	109	124	138	163	190	215	235	258	271	275	273	266	260	249	234	215	193	171	156	144	133	123	113	104	90
34	90	90	94	100	109	124	137	163	190	215	235	258	271	275	273	267	260	249	234	215	193	172	156	144	133	123	113	104	90
35	90	90	94	99	109	124	137	163	190	215	234	258	270	275	273	267	260	249	234	215	193	172	156	144	133	123	113	104	90
36	90	90	94	99	109	124	137	163	190	215	234	258	270	275	273	267	260	249	234	215	193	172	156	144	133	123	113	104	90

Table 5. Geochemical modeling results for albite - test 13

Table 6. Geochemical modeling results for K-feldspar - test 13

Table 7. Geochemical modeling results for montmorillonite - test 13

Table 7...continued. Geochemical modeling results for montmorillonite - test 13

Table 8. Geochemical modeling results for quartz - test 13

Table 9. Geochemical modeling results for porosity - test 13

Table 9...continued. Geochemical modeling results for porosity - test 13

Table 10. Geochemical modeling results for temperature - test 14 (blue = sill; red = 10% sandstone)

		Depth	Time	0	10	34	50	71	100	126	150	165	193	200	229	261	299	300	383	400	542	600	1001	10007	3,2E+11
				0	3,2E+00	1,1E+09	1,6E+09	2,2E+09	3,2E+09	4,0E+09	4,7E+09	5,2E+09	6,1E+09	6,3E+09	7,2E+09	8,2E+09	9,4E+09	9,5E+09	1,2E+10	1,3E+10	1,7E+10	1,9E+10	3,2E+10	90	
0		90	95	110	120	132	150	176	200	215	242	250	221	189	151	150	125	120	99	99	90	90	90	90	
1		90	95	110	120	132	150	176	200	215	242	250	221	189	151	150	125	120	99	99	90	90	90	90	
2		90	95	110	120	132	150	176	200	215	242	250	221	189	151	150	125	120	99	90	90	90	90	90	
3		90	95	110	120	132	150	176	200	215	242	250	221	189	151	150	125	120	99	90	90	90	90	90	
4		90	94	108	118	130	148	173	196	211	239	246	222	191	154	153	127	121	99	91	90	90	90	90	
5		90	94	107	117	129	146	170	193	208	235	242	222	193	157	156	128	123	100	91	90	90	90	90	
6		90	93	106	115	127	144	167	190	204	231	239	222	194	159	159	129	124	101	92	90	90	90	90	
7		90	93	105	114	125	142	164	187	201	228	235	221	196	162	161	131	126	101	92	90	90	90	90	
8		90	93	104	112	123	140	162	184	198	225	232	221	197	165	164	132	127	102	93	90	90	90	90	
9		90	92	103	111	122	138	159	181	195	221	229	221	199	167	166	134	128	103	94	90	90	90	90	
10		90	92	102	110	120	136	157	178	192	218	225	221	200	169	169	135	129	103	94	90	90	90	90	
11		90	92	101	109	119	135	154	175	189	215	222	220	201	171	171	136	130	104	95	90	90	90	90	
12		90	91	100	107	118	133	152	173	187	212	220	220	202	174	173	137	132	104	95	90	90	90	90	
13		90	91	99	106	116	132	150	171	184	210	217	219	203	176	175	138	133	105	96	90	90	90	90	
14		90	91	98	105	115	130	148	168	182	207	214	219	204	177	177	140	134	105	96	90	90	90	90	
15		90	91	98	104	114	129	147	166	180	205	212	218	205	179	179	141	135	106	96	90	90	90	90	
16		90	91	97	104	113	128	145	164	177	202	209	217	206	181	180	142	136	106	97	90	90	90	90	
17		90	91	97	103	112	126	143	162	175	200	207	217	207	182	182	143	137	107	97	90	90	90	90	
18		90	90	96	102	111	125	142	160	173	198	205	216	207	184	183	143	137	107	98	90	90	90	90	
19		90	90	96	101	110	124	140	159	172	196	203	215	208	185	185	144	138	107	98	90	90	90	90	
20		90	90	95	101	109	123	139	157	170	194	201	215	209	187	186	145	139	108	98	90	90	90	90	
21		90	90	95	100	108	122	138	156	168	192	199	214	209	188	187	146	140	108	99	90	90	90	90	
22		90	90	94	99	107	121	136	154	167	191	198	213	210	189	189	147	140	108	99	90	90	90	90	
23		90	90	94	99	107	120	135	153	165	189	196	213	210	190	190	147	141	109	99	90	90	90	90	
24		90	90	94	98	106	120	134	152	164	188	195	212	210	191	191	148	142	109	99	90	90	90	90	
25		90	90	93	98	106	119	134	151	163	187	194	212	211	192	191	149	142	109	100	90	90	90	90	
26		90	90	93	98	105	118	133	150	162	186	192	211	211	193	192	149	143	109	100	90	90	90	90	
27		90	90	93	97	105	118	132	149	161	185	191	211	211	193	193	150	143	110	100	90	90	90	90	
28		90	90	93	97	104	117	131	148	160	184	190	210	211	194	194	150	143	110	100	90	90	90	90	
29		90	90	93	97	104	117	131	147	159	183	190	210	212	195	194	150	144	110	100	90	90	90	90	
30		90	90	92	96	104	117	130	147	159	182	189	210	212	195	195	151	144	110	100	90	90	90	90	
31		90	90	92	96	103	116	130	146	158	182	188	209	212	195	195	151	144	110	101	90	90	90	90	
32		90	90	92	96	103	116	130	146	158	181	188	209	212	196	195	151	145	110	101	90	90	90	90	
33		90	90	92	96	103	116	129	146	157	181	187	209	212	196	196	151	145	110	101	90	90	90	90	
34		90	90	92	96	103	116	129	145	157	180	187	209	212	196	196	151	145	110	101	90	90	90	90	
35		90	90	92	96	103	116	129	145	157	180	187	209	212	196	196	151	145	110	101	90	90	90	90	

Table 11. Geochemical modeling results for albite - test 14

Table 12. Geochemical modeling results for K-feldspar - test 14

Table 13. Geochemical modeling results for montmorillonite - test 14

Table 14. Geochemical modeling results for quartz - test 14

Table 14...continued. Geochemical modeling results for quartz - test 14

Table 15. Geochemical modeling results for porosity - test 14

K+		Depth	Time	K+ concentration (ppm)																										
				0,0E+00	10	32	1,0E+09	1,6E+09	79	2,5E+09	100	3,2E+09	126	4,0E+09	150	4,7E+09	165	5,2E+09	190	6,0E+09	200	6,3E+09	228	7,2E+09	244	7,7E+09	261	8,2E+09	279	8,8E+09
0	2,307E-06	4,572E-06	3,943E-06	2,192E-06	5,174E-07	3,029E-07	1,790E-07	1,013E-07	5,167E-08	2,142E-08	7,542E-09	1,195E-05	1,202E-05	1,033E-05	1,017E-05	1,278E-05														
1	2,307E-06	1,506E-08	1,912E-08	2,507E-08	3,773E-08	5,109E-08	7,254E-08	9,897E-08	1,066E-07	1,188E-07	1,241E-07	3,858E-06	4,134E-06	4,054E-06	3,749E-06	3,359E-06														
2	2,307E-06	2,427E-06	3,290E-06	4,108E-06	5,760E-06	7,424E-06	1,079E-05	1,528E-05	1,812E-05	2,386E-05	2,686E-05	1,957E-05	1,646E-05	1,319E-05	1,015E-05	7,605E-06														
3	2,307E-06	1,133E-05	3,430E-05	6,540E-05	1,538E-04	2,742E-04	6,361E-04	1,367E-03	2,734E-03	9,058E-03	1,271E-02	1,109E-07	1,037E-07	8,795E-08	6,894E-08	5,317E-08														
4	2,307E-06	7,129E-06	1,325E-05	1,738E-05	2,603E-05	3,450E-05	4,991E-05	6,556E-05	7,921E-05	8,750E-05	8,905E-05	2,537E-05	2,890E-05	2,655E-05	2,148E-05	1,694E-05														
5	2,307E-06	2,627E-06	3,732E-06	4,761E-06	7,012E-06	9,423E-06	1,349E-05	1,861E-05	2,111E-05	2,401E-05	2,556E-05	2,404E-05	2,306E-05	2,177E-05	1,798E-05	1,369E-05														
6	2,307E-06	2,577E-06	3,628E-06	4,590E-06	6,712E-06	8,989E-06	1,300E-05	1,782E-05	2,086E-05	2,353E-05	2,502E-05	2,395E-05	2,239E-05	2,016E-05	1,682E-05	1,317E-05														
7	2,307E-06	2,533E-06	3,535E-06	4,435E-06	6,443E-06	8,603E-06	1,258E-05	1,713E-05	2,072E-05	2,310E-05	2,449E-05	2,385E-05	2,239E-05	2,001E-05	1,634E-05	1,311E-05														
8	2,307E-06	2,494E-06	3,460E-06	4,313E-06	6,233E-06	8,304E-06	1,230E-05	1,659E-05	2,023E-05	2,268E-05	2,389E-05	2,367E-05	2,239E-05	2,033E-05	1,635E-05	1,313E-05														
9	2,307E-06	2,508E-06	3,521E-06	4,353E-06	6,228E-06	8,263E-06	1,232E-05	1,626E-05	1,966E-05	2,219E-05	2,314E-05	2,333E-05	2,256E-05	2,118E-05	1,687E-05	1,319E-05														
10	2,307E-06	2,475E-06	3,441E-06	4,219E-06	5,992E-06	7,924E-06	1,197E-05	1,568E-05	1,890E-05	2,194E-05	2,282E-05	2,318E-05	2,254E-05	2,149E-05	1,738E-05	1,355E-05														
11	2,307E-06	2,447E-06	3,369E-06	4,096E-06	5,775E-06	7,613E-06	1,164E-05	1,515E-05	1,821E-05	2,172E-05	2,254E-05	2,304E-05	2,250E-05	2,154E-05	1,782E-05	1,397E-05														
12	2,307E-06	2,423E-06	3,264E-06	3,983E-06	5,576E-06	7,326E-06	1,135E-05	1,466E-05	1,757E-05	2,152E-05	2,228E-05	2,290E-05	2,245E-05	2,159E-05	1,824E-05	1,440E-05														
13	2,307E-06	2,401E-06	3,167E-06	3,879E-06	5,392E-06	7,063E-06	1,108E-05	1,421E-05	1,698E-05	2,135E-05	2,205E-05	2,277E-05	2,241E-05	2,163E-05	1,865E-05	1,481E-05														
14	2,307E-06	2,383E-06	3,080E-06	3,785E-06	5,224E-06	6,821E-06	1,060E-05	1,380E-05	1,644E-05	2,119E-05	2,184E-05	2,264E-05	2,237E-05	2,167E-05	1,905E-05	1,522E-05														
15	2,307E-06	2,368E-06	3,002E-06	3,698E-06	5,069E-06	6,598E-06	1,014E-05	1,342E-05	1,595E-05	2,107E-05	2,164E-05	2,251E-05	2,232E-05	2,171E-05	1,942E-05	1,561E-05														
16	2,307E-06	2,354E-06	2,931E-06	3,619E-06	4,926E-06	6,394E-06	9,718E-06	1,308E-05	1,550E-05	2,086E-05	2,148E-05	2,240E-05	2,227E-05	2,173E-05	1,977E-05	1,598E-05														
17	2,307E-06	2,343E-06	2,866E-06	3,547E-06	4,796E-06	6,206E-06	9,337E-06	1,276E-05	1,508E-05	2,024E-05	2,134E-05	2,229E-05	2,223E-05	2,175E-05	2,012E-05	1,634E-05														
18	2,307E-06	2,333E-06	2,808E-06	3,481E-06	4,676E-06	6,035E-06	8,994E-06	1,248E-05	1,470E-05	1,968E-05	2,121E-05	2,218E-05	2,218E-05	2,177E-05	2,045E-05	1,669E-05														
19	2,307E-06	2,325E-06	2,757E-06	3,421E-06	4,566E-06	5,877E-06	8,683E-06	1,222E-05	1,435E-05	1,917E-05	2,109E-05	2,208E-05	2,214E-05	2,179E-05	2,077E-05	1,704E-05														
20	2,307E-06	2,318E-06	2,709E-06	3,367E-06	4,466E-06	5,734E-06	8,402E-06	1,198E-05	1,403E-05	1,869E-05	2,100E-05	2,199E-05	2,210E-05	2,181E-05	2,107E-05	1,737E-05														
21	2,307E-06	2,312E-06	2,666E-06	3,314E-06	4,375E-06	5,603E-06	8,150E-06	1,176E-05	1,375E-05	1,826E-05	2,077E-05	2,191E-05	2,206E-05	2,182E-05	2,114E-05	1,767E-05														
22	2,307E-06	2,308E-06	2,628E-06	3,241E-06	4,292E-06	5,483E-06	7,922E-06	1,157E-05	1,349E-05	1,787E-05	2,031E-05	2,184E-05	2,203E-05	2,184E-05	2,119E-05	1,796E-05														
23	2,307E-06	2,304E-06	2,594E-06	3,176E-06	4,217E-06	5,375E-06	7,718E-06	1,139E-05	1,325E-05	1,751E-05	1,990E-05	2,176E-05	2,199E-05	2,185E-05	2,125E-05	1,824E-05														
24	2,307E-06	2,300E-06	2,564E-06	3,117E-06	4,149E-06	5,277E-06	7,535E-06	1,124E-05	1,304E-05	1,719E-05	1,951E-05	2,170E-05	2,196E-05	2,186E-05	2,130E-05	1,850E-05														
25	2,307E-06	2,298E-06	2,537E-06	3,064E-06	4,088E-06	5,190E-06	7,372E-06	1,110E-05	1,285E-05	1,691E-05	1,918E-05	2,165E-05	2,193E-05	2,187E-05	2,135E-05	1,873E-05														
26	2,307E-06	2,295E-06	2,513E-06	3,017E-06	4,034E-06	5,112E-06	7,228E-06	1,093E-05	1,268E-05	1,665E-05	1,888E-05	2,160E-05	2,191E-05	2,188E-05	2,139E-05	1,895E-05														
27	2,307E-06	2,294E-06	2,492E-06	2,976E-06	3,986E-06	5,042E-06	7,101E-06	1,070E-05	1,253E-05	1,643E-05	1,862E-05	2,155E-05	2,189E-05	2,188E-05	2,143E-05	1,916E-05														
28	2,307E-06	2,292E-06	2,474E-06	2,940E-06	3,944E-06	4,982E-06	6,991E-06	1,049E-05	1,240E-05	1,623E-05	1,838E-05	2,151E-05	2,186E-05	2,189E-05	2,146E-05	1,933E-05														
29	2,307E-06	2,291E-06	2,458E-06	2,910E-06	3,908E-06	4,929E-06	6,896E-06	1,032E-05	1,229E-05	1,606E-05	1,818E-05	2,148E-05	2,185E-05	2,189E-05	2,149E-05	1,950E-05														
30	2,307E-06	2,290E-06	2,445E-06	2,884E-06	3,877E-06	4,885E-06	6,816E-06	1,018E-05	1,219E-05	1,591E-05	1,801E-05	2,145E-05	2,183E-05	2,190E-05	2,151E-05	1,963E-05														
31	2,307E-06	2,290E-06	2,434E-06	2,862E-06	3,852E-06	4,849E-06	6,750E-06	1,006E-05	1,211E-05	1,579E-05	1,786E-05	2,143E-05	2,182E-05	2,190E-05	2,153E-05	1,975E-05														
32	2,307E-06	2,289E-06	2,426E-06	2,845E-06	3,832E-06	4,820E-06	6,698E-06	9,961E-06	1,205E-05	1,569E-05	1,776E-05	2,141E-05	2,181E-05	2,190E-05	2,155E-05	1,984E-05														
33	2,307E-06	2,289E-06	2,419E-06	2,833E-06	3,817E-06	4,798E-06	6,659E-06	9,890E-06	1,201E-05	1,563E-05	1,768E-05	2,140E-05	2,180E-05	2,190E-05	2,156E-05	1,990E-05														
34	2,307E-06	2,288E-06	2,415E-06	2,824E-06	3,807E-06	4,783E-06	6,634E-06	9,843E-06	1,198E-05	1,558E-05	1,762E-05	2,139E-05	2,180E-05	2,191E-05	2,156E-05	1,995E-05														
35	2,307E-06	2,288E-06	2,413E-06	2,820E-06	3,802E-06	4,776E-06																								

Table 16...continued. Geochemical modeling results for potassium - test 14

	336 1,1E+10	379 1,2E+10	400 1,3E+10	467 1,5E+10	542 1,7E+10	600 1,9E+10	1001 3,2E+10	7455 2,4E+11	10007 3,2E+11
3,155E-06	4,099E-06	4,398E-06	3,430E-06	3,143E-06	2,696E-06	2,309E-06	2,309E-06	2,309E-06	2,309E-06
3,254E-06	3,043E-06	2,908E-06	2,962E-06	2,871E-06	2,596E-06	4,759E-06	2,954E-05	4,322E-05	
5,997E-06	4,666E-06	4,109E-06	3,377E-06	2,685E-06	2,127E-06	2,127E-06	2,127E-06	2,127E-06	
3,946E-08	2,958E-08	2,531E-08	1,993E-08	1,507E-08	1,078E-08	1,059E-08	1,067E-08	1,072E-08	
1,153E-05	7,463E-06	6,159E-06	4,329E-06	3,152E-06	2,275E-06	2,112E-06	2,112E-06	2,112E-06	
9,413E-06	6,361E-06	5,340E-06	3,987E-06	3,006E-06	2,193E-06	2,113E-06	2,113E-06	2,113E-06	
9,337E-06	6,384E-06	5,381E-06	4,034E-06	3,046E-06	2,236E-06	2,118E-06	2,118E-06	2,118E-06	
9,723E-06	6,669E-06	5,611E-06	4,153E-06	3,117E-06	2,298E-06	2,130E-06	2,130E-06	2,130E-06	
1,017E-05	7,014E-06	5,898E-06	4,303E-06	3,208E-06	2,374E-06	2,154E-06	2,154E-06	2,154E-06	
1,038E-05	7,143E-06	6,032E-06	4,435E-06	3,321E-06	2,458E-06	2,236E-06	2,235E-06	2,235E-06	
1,043E-05	7,242E-06	6,115E-06	4,499E-06	3,390E-06	2,537E-06	2,279E-06	2,278E-06	2,278E-06	
1,058E-05	7,373E-06	6,202E-06	4,516E-06	3,407E-06	2,571E-06	2,276E-06	2,275E-06	2,275E-06	
1,079E-05	7,551E-06	6,321E-06	4,539E-06	3,412E-06	2,589E-06	2,254E-06	2,254E-06	2,254E-06	
1,102E-05	7,760E-06	6,469E-06	4,582E-06	3,429E-06	2,612E-06	2,235E-06	2,235E-06	2,235E-06	
1,124E-05	7,975E-06	6,627E-06	4,636E-06	3,456E-06	2,645E-06	2,224E-06	2,224E-06	2,224E-06	
1,147E-05	8,196E-06	6,787E-06	4,693E-06	3,488E-06	2,682E-06	2,220E-06	2,219E-06	2,219E-06	
1,168E-05	8,412E-06	6,944E-06	4,754E-06	3,522E-06	2,720E-06	2,218E-06	2,217E-06	2,217E-06	
1,190E-05	8,627E-06	7,099E-06	4,815E-06	3,556E-06	2,758E-06	2,217E-06	2,217E-06	2,217E-06	
1,210E-05	8,844E-06	7,253E-06	4,870E-06	3,590E-06	2,796E-06	2,217E-06	2,217E-06	2,217E-06	
1,230E-05	9,048E-06	7,400E-06	4,924E-06	3,619E-06	2,831E-06	2,218E-06	2,217E-06	2,217E-06	
1,250E-05	9,251E-06	7,543E-06	4,975E-06	3,648E-06	2,866E-06	2,218E-06	2,217E-06	2,217E-06	
1,269E-05	9,452E-06	7,680E-06	5,024E-06	3,676E-06	2,899E-06	2,218E-06	2,217E-06	2,217E-06	
1,286E-05	9,641E-06	7,809E-06	5,070E-06	3,702E-06	2,931E-06	2,218E-06	2,217E-06	2,217E-06	
1,303E-05	9,819E-06	7,937E-06	5,114E-06	3,727E-06	2,960E-06	2,218E-06	2,217E-06	2,217E-06	
1,320E-05	9,991E-06	8,056E-06	5,156E-06	3,749E-06	2,987E-06	2,218E-06	2,217E-06	2,217E-06	
1,334E-05	1,011E-05	8,168E-06	5,194E-06	3,770E-06	3,013E-06	2,218E-06	2,217E-06	2,217E-06	
1,347E-05	1,019E-05	8,271E-06	5,230E-06	3,789E-06	3,036E-06	2,218E-06	2,217E-06	2,217E-06	
1,361E-05	1,025E-05	8,359E-06	5,260E-06	3,807E-06	3,058E-06	2,218E-06	2,217E-06	2,217E-06	
1,371E-05	1,031E-05	8,447E-06	5,290E-06	3,822E-06	3,072E-06	2,218E-06	2,217E-06	2,217E-06	
1,381E-05	1,037E-05	8,524E-06	5,312E-06	3,835E-06	3,081E-06	2,218E-06	2,217E-06	2,217E-06	
1,390E-05	1,042E-05	8,586E-06	5,337E-06	3,847E-06	3,089E-06	2,218E-06	2,217E-06	2,217E-06	
1,396E-05	1,046E-05	8,642E-06	5,359E-06	3,857E-06	3,097E-06	2,218E-06	2,217E-06	2,217E-06	
1,404E-05	1,049E-05	8,686E-06	5,370E-06	3,865E-06	3,102E-06	2,218E-06	2,217E-06	2,217E-06	
1,408E-05	1,052E-05	8,722E-06	5,383E-06	3,870E-06	3,105E-06	2,218E-06	2,217E-06	2,217E-06	
1,410E-05	1,053E-05	8,745E-06	5,388E-06	3,874E-06	3,110E-06	2,218E-06	2,217E-06	2,217E-06	
1,412E-05	1,054E-05	8,756E-06	5,391E-06	3,876E-06	3,112E-06	2,217E-06	2,216E-06	2,216E-06	
1,772E-05	1,283E-05	1,027E-05	5,884E-06	4,027E-06	3,085E-06	2,136E-06	2,135E-06	2,135E-06	

Table 17. Geochemical modeling results for aluminium - test 14

Al+++		Depth	Time	Al+++																									
0,0E+00	0,0E+00			10	32	1,0E+09	1,6E+09	50	79	100	3,2E+09	126	4,0E+09	150	4,7E+09	165	5,2E+09	190	6,0E+09	200	6,3E+09	228	7,2E+09	244	7,7E+09	261	8,2E+09	279	8,8E+09
0	1,051E-12	1,887E-12	1,341E-12	6,395E-13	1,180E-13	5,757E-14	2,411E-14	9,800E-15	4,084E-15	1,210E-15	3,793E-16	9,458E-13	1,123E-12	1,181E-12	1,471E-12	2,396E-12													
1	1,051E-12	1,531E-06	1,959E-06	2,075E-06	2,257E-06	2,405E-06	2,402E-06	2,389E-06	2,221E-06	1,958E-06	1,851E-06	5,859E-13	4,871E-13	3,679E-13	2,639E-13	1,961E-13													
2	1,051E-12	1,453E-12	2,172E-12	2,737E-12	3,884E-12	5,042E-12	5,058E-12	5,033E-12	3,810E-12	2,379E-12	1,936E-12	3,344E-12	4,484E-12	5,045E-12	5,055E-12	5,042E-12													
3	1,051E-12	1,476E-14	2,156E-15	8,326E-16	2,966E-16	1,675E-16	5,862E-17	2,404E-17	7,888E-18	1,110E-18	6,033E-19	2,139E-06	2,308E-06	2,387E-06	2,400E-06	2,405E-06													
4	1,051E-12	3,074E-12	4,707E-12	5,270E-12	6,182E-12	6,811E-12	7,109E-12	6,872E-12	7,014E-12	5,983E-12	5,454E-12	2,007E-12	2,669E-12	2,963E-12	3,008E-12	3,052E-12													
5	1,051E-12	1,139E-12	1,348E-12	1,476E-12	1,711E-12	1,917E-12	1,996E-12	2,036E-12	1,939E-12	1,706E-12	1,628E-12	1,900E-12	2,107E-12	2,373E-12	2,442E-12	2,377E-12													
6	1,051E-12	1,126E-12	1,334E-12	1,455E-12	1,683E-12	1,882E-12	1,995E-12	2,033E-12	1,986E-12	1,737E-12	1,656E-12	1,895E-12	2,026E-12	2,150E-12	2,217E-12	2,206E-12													
7	1,051E-12	1,114E-12	1,320E-12	1,436E-12	1,657E-12	1,853E-12	2,000E-12	2,035E-12	2,041E-12	1,769E-12	1,682E-12	1,890E-12	2,008E-12	2,092E-12	2,094E-12	2,123E-12													
8	1,051E-12	1,103E-12	1,312E-12	1,425E-12	1,644E-12	1,837E-12	2,022E-12	2,048E-12	2,070E-12	1,799E-12	1,701E-12	1,880E-12	1,994E-12	2,085E-12	2,039E-12	2,057E-12													
9	1,051E-12	1,116E-12	1,355E-12	1,466E-12	1,682E-12	1,877E-12	2,094E-12	2,084E-12	2,092E-12	1,821E-12	1,705E-12	1,859E-12	1,996E-12	2,134E-12	2,051E-12	2,002E-12													
10	1,051E-12	1,106E-12	1,342E-12	1,447E-12	1,655E-12	1,845E-12	2,097E-12	2,082E-12	2,089E-12	1,859E-12	1,738E-12	1,856E-12	1,982E-12	2,132E-12	2,064E-12	1,997E-12													
11	1,051E-12	1,098E-12	1,331E-12	1,429E-12	1,631E-12	1,816E-12	2,101E-12	2,081E-12	2,087E-12	1,899E-12	1,772E-12	1,853E-12	1,969E-12	2,110E-12	2,068E-12	2,001E-12													
12	1,051E-12	1,091E-12	1,305E-12	1,413E-12	1,607E-12	1,788E-12	2,106E-12	2,080E-12	2,084E-12	1,938E-12	1,806E-12	1,852E-12	1,957E-12	2,091E-12	2,072E-12	2,007E-12													
13	1,051E-12	1,085E-12	1,281E-12	1,398E-12	1,585E-12	1,761E-12	2,112E-12	2,080E-12	2,081E-12	1,978E-12	1,839E-12	1,852E-12	1,947E-12	2,073E-12	2,077E-12	2,012E-12													
14	1,051E-12	1,080E-12	1,259E-12	1,383E-12	1,565E-12	1,737E-12	2,078E-12	2,080E-12	2,079E-12	2,018E-12	1,873E-12	1,853E-12	1,938E-12	2,056E-12	2,080E-12	2,017E-12													
15	1,051E-12	1,075E-12	1,239E-12	1,370E-12	1,546E-12	1,714E-12	2,040E-12	2,081E-12	2,078E-12	2,059E-12	1,907E-12	1,855E-12	1,930E-12	2,042E-12	2,083E-12	2,022E-12													
16	1,051E-12	1,071E-12	1,221E-12	1,358E-12	1,528E-12	1,692E-12	2,005E-12	2,082E-12	2,077E-12	2,092E-12	1,940E-12	1,858E-12	1,923E-12	2,027E-12	2,087E-12	2,026E-12													
17	1,051E-12	1,068E-12	1,204E-12	1,347E-12	1,511E-12	1,672E-12	1,972E-12	2,083E-12	2,076E-12	2,088E-12	1,974E-12	1,862E-12	1,917E-12	2,014E-12	2,091E-12	2,030E-12													
18	1,051E-12	1,065E-12	1,189E-12	1,337E-12	1,496E-12	1,653E-12	1,942E-12	2,085E-12	2,076E-12	2,086E-12	2,006E-12	1,867E-12	1,912E-12	2,002E-12	2,094E-12	2,033E-12													
19	1,051E-12	1,063E-12	1,175E-12	1,328E-12	1,481E-12	1,635E-12	1,914E-12	2,087E-12	2,075E-12	2,084E-12	2,038E-12	1,872E-12	1,908E-12	1,991E-12	2,098E-12	2,039E-12													
20	1,051E-12	1,061E-12	1,162E-12	1,320E-12	1,468E-12	1,619E-12	1,889E-12	2,075E-12	2,082E-12	2,070E-12	1,877E-12	1,905E-12	1,982E-12	2,102E-12	2,043E-12														
21	1,051E-12	1,059E-12	1,151E-12	1,311E-12	1,456E-12	1,604E-12	1,865E-12	2,092E-12	2,075E-12	2,080E-12	2,089E-12	1,883E-12	1,902E-12	1,973E-12	2,089E-12	2,046E-12													
22	1,051E-12	1,057E-12	1,140E-12	1,293E-12	1,445E-12	1,590E-12	1,844E-12	2,095E-12	2,076E-12	2,079E-12	2,087E-12	1,890E-12	1,900E-12	1,965E-12	2,076E-12	2,050E-12													
23	1,051E-12	1,056E-12	1,131E-12	1,277E-12	1,435E-12	1,578E-12	1,824E-12	2,098E-12	2,077E-12	2,077E-12	2,085E-12	1,896E-12	1,898E-12	1,958E-12	2,065E-12	2,053E-12													
24	1,051E-12	1,055E-12	1,123E-12	1,263E-12	1,425E-12	1,566E-12	1,807E-12	2,101E-12	2,077E-12	2,076E-12	2,083E-12	1,902E-12	1,897E-12	1,951E-12	2,056E-12	2,057E-12													
25	1,051E-12	1,055E-12	1,115E-12	1,249E-12	1,417E-12	1,556E-12	1,791E-12	2,104E-12	2,078E-12	2,075E-12	2,082E-12	1,909E-12	1,897E-12	1,946E-12	2,047E-12	2,060E-12													
26	1,051E-12	1,054E-12	1,109E-12	1,238E-12	1,409E-12	1,546E-12	1,776E-12	2,100E-12	2,079E-12	2,074E-12	2,081E-12	1,915E-12	1,896E-12	1,941E-12	2,039E-12	2,063E-12													
27	1,051E-12	1,053E-12	1,103E-12	1,227E-12	1,403E-12	1,538E-12	1,763E-12	2,082E-12	2,080E-12	2,074E-12	2,080E-12	1,921E-12	1,896E-12	1,937E-12	2,031E-12	2,067E-12													
28	1,051E-12	1,053E-12	1,098E-12	1,218E-12	1,397E-12	1,530E-12	1,752E-12	2,066E-12	2,081E-12	2,073E-12	2,079E-12	1,927E-12	1,896E-12	1,933E-12	2,025E-12	2,069E-12													
29	1,051E-12	1,053E-12	1,094E-12	1,211E-12	1,392E-12	1,524E-12	1,743E-12	2,052E-12	2,082E-12	2,073E-12	2,078E-12	1,932E-12	1,896E-12	1,930E-12	2,019E-12	2,072E-12													
30	1,051E-12	1,052E-12	1,090E-12	1,204E-12	1,387E-12	1,518E-12	1,734E-12	2,040E-12	2,083E-12	2,072E-12	2,077E-12	1,936E-12	1,896E-12	1,927E-12	2,015E-12	2,074E-12													
31	1,051E-12	1,052E-12	1,087E-12	1,198E-12	1,384E-12	1,514E-12	1,727E-12	2,030E-12	2,084E-12	2,071E-12	2,076E-12	1,940E-12	1,896E-12	1,925E-12	2,011E-12	2,075E-12													
32	1,051E-12	1,052E-12	1,084E-12	1,194E-12	1,381E-12	1,510E-12	1,722E-12	2,022E-12	2,085E-12	2,071E-12	2,076E-12	1,944E-12	1,896E-12	1,923E-12	2,008E-12	2,077E-12													
33	1,051E-12	1,052E-12	1,083E-12	1,191E-12	1,379E-12	1,508E-12	1,718E-12	2,017E-12	2,085E-12	2,072E-12	2,076E-12	1,946E-12	1,897E-12	1,922E-12	2,005E-12	2,077E-12													
34	1,051E-12	1,052E-12	1,081E-12	1,189E-12	1,378E-12	1,506E-12	1,715E-12	2,013E-12	2,086E-12	2,072E-12	2,076E-12	1,947E-12	1,897E-12	1,921E-12	2,004E-12	2,079E-12													
35	1,051E-12	1,052E-12	1,081E-12	1,188E-12	1,377E																								

Table 17...continued. Geochemical modeling results for aluminium - test 14

336 1,1E+10	379 1,2E+10	400 1,3E+10	467 1,5E+10	542 1,7E+10	600 1,9E+10	1001 3,2E+10	7455 2,4E+11	10007 3,2E+11
7,048E-13	1,105E-12	1,303E-12	1,173E-12	1,267E-12	1,241E-12	1,062E-12	1,062E-12	1,062E-12
1,120E-13	6,508E-14	5,064E-14	3,060E-14	1,806E-14	1,030E-14	4,735E-15	2,115E-16	9,292E-17
4,046E-12	3,122E-12	2,736E-12	2,230E-12	1,719E-12	1,161E-12	1,162E-12	1,162E-12	1,162E-12
2,277E-06	2,146E-06	2,080E-06	1,980E-06	1,869E-06	1,686E-06	1,657E-06	1,646E-06	1,638E-06
2,512E-12	1,965E-12	1,783E-12	1,460E-12	1,254E-12	1,036E-12	9,708E-13	9,707E-13	9,707E-13
1,996E-12	1,639E-12	1,515E-12	1,329E-12	1,185E-12	9,887E-13	9,712E-13	9,712E-13	9,712E-13
1,928E-12	1,610E-12	1,496E-12	1,329E-12	1,189E-12	9,990E-13	9,733E-13	9,733E-13	9,733E-13
1,957E-12	1,648E-12	1,531E-12	1,353E-12	1,206E-12	1,018E-12	9,790E-13	9,789E-13	9,789E-13
1,995E-12	1,698E-12	1,579E-12	1,387E-12	1,231E-12	1,042E-12	9,900E-13	9,899E-13	9,899E-13
1,987E-12	1,696E-12	1,586E-12	1,414E-12	1,263E-12	1,070E-12	1,028E-12	1,028E-12	1,028E-12
1,954E-12	1,687E-12	1,580E-12	1,419E-12	1,279E-12	1,096E-12	1,047E-12	1,047E-12	1,047E-12
1,942E-12	1,687E-12	1,575E-12	1,411E-12	1,275E-12	1,102E-12	1,046E-12	1,046E-12	1,046E-12
1,941E-12	1,697E-12	1,579E-12	1,404E-12	1,268E-12	1,101E-12	1,036E-12	1,036E-12	1,036E-12
1,944E-12	1,715E-12	1,591E-12	1,404E-12	1,265E-12	1,103E-12	1,027E-12	1,027E-12	1,027E-12
1,947E-12	1,734E-12	1,606E-12	1,408E-12	1,266E-12	1,110E-12	1,022E-12	1,022E-12	1,022E-12
1,950E-12	1,754E-12	1,621E-12	1,413E-12	1,269E-12	1,118E-12	1,020E-12	1,020E-12	1,020E-12
1,953E-12	1,774E-12	1,636E-12	1,420E-12	1,273E-12	1,127E-12	1,019E-12	1,019E-12	1,019E-12
1,956E-12	1,793E-12	1,650E-12	1,426E-12	1,278E-12	1,136E-12	1,019E-12	1,019E-12	1,019E-12
1,958E-12	1,813E-12	1,665E-12	1,432E-12	1,282E-12	1,145E-12	1,019E-12	1,019E-12	1,019E-12
1,961E-12	1,832E-12	1,679E-12	1,437E-12	1,286E-12	1,153E-12	1,019E-12	1,019E-12	1,019E-12
1,964E-12	1,850E-12	1,692E-12	1,443E-12	1,290E-12	1,162E-12	1,019E-12	1,019E-12	1,019E-12
1,967E-12	1,869E-12	1,705E-12	1,448E-12	1,293E-12	1,170E-12	1,019E-12	1,019E-12	1,019E-12
1,970E-12	1,886E-12	1,717E-12	1,452E-12	1,296E-12	1,178E-12	1,019E-12	1,019E-12	1,019E-12
1,972E-12	1,901E-12	1,729E-12	1,457E-12	1,300E-12	1,184E-12	1,019E-12	1,019E-12	1,019E-12
1,976E-12	1,917E-12	1,740E-12	1,461E-12	1,303E-12	1,191E-12	1,019E-12	1,019E-12	1,019E-12
1,977E-12	1,924E-12	1,751E-12	1,465E-12	1,305E-12	1,197E-12	1,019E-12	1,019E-12	1,019E-12
1,978E-12	1,925E-12	1,760E-12	1,469E-12	1,307E-12	1,202E-12	1,019E-12	1,019E-12	1,019E-12
1,982E-12	1,925E-12	1,768E-12	1,471E-12	1,310E-12	1,208E-12	1,019E-12	1,019E-12	1,019E-12
1,983E-12	1,925E-12	1,776E-12	1,475E-12	1,312E-12	1,210E-12	1,019E-12	1,019E-12	1,019E-12
1,984E-12	1,927E-12	1,783E-12	1,476E-12	1,313E-12	1,211E-12	1,019E-12	1,019E-12	1,019E-12
1,985E-12	1,928E-12	1,789E-12	1,479E-12	1,315E-12	1,212E-12	1,019E-12	1,019E-12	1,019E-12
1,985E-12	1,928E-12	1,794E-12	1,482E-12	1,316E-12	1,214E-12	1,019E-12	1,019E-12	1,019E-12
1,988E-12	1,929E-12	1,798E-12	1,483E-12	1,317E-12	1,214E-12	1,019E-12	1,019E-12	1,019E-12
1,989E-12	1,931E-12	1,802E-12	1,484E-12	1,317E-12	1,214E-12	1,019E-12	1,019E-12	1,019E-12
1,988E-12	1,930E-12	1,804E-12	1,484E-12	1,318E-12	1,216E-12	1,019E-12	1,019E-12	1,019E-12
1,989E-12	1,931E-12	1,805E-12	1,485E-12	1,318E-12	1,216E-12	1,019E-12	1,019E-12	1,019E-12
2,496E-12	2,350E-12	2,118E-12	1,621E-12	1,370E-12	1,206E-12	9,816E-13	9,814E-13	9,815E-13

Table 18. Geochemical modeling results for SiO_2 aqueous - test 14

Depth	Time	SiO2 aqua																		
		0,0E+00	3,2E+08	1,0E+09	1,6E+09	2,5E+09	3,2E+09	4,0E+09	4,7E+09	5,2E+09	6,0E+09	6,3E+09	7,2E+09	7,7E+09	8,2E+09	8,8E+09	9,4E+09	1,1E+10	1,2E+10	1,3E+10
		0	10	32	50	79	100	126	150	165	190	200	228	244	261	279	299	336	379	400
0	0,0007	0,0008	0,0010	0,0012	0,0016	0,0019	0,0027	0,0036	0,0043	0,0056	0,0062	0,0046	0,0039	0,0032	0,0025	0,0019	0,0016	0,0013	0,0012	
1	0,0007	0,0007	0,0010	0,0012	0,0015	0,0019	0,0027	0,0036	0,0043	0,0056	0,0062	0,0046	0,0039	0,0032	0,0025	0,0020	0,0016	0,0013	0,0012	
2	0,0007	0,0007	0,0010	0,0012	0,0015	0,0019	0,0027	0,0036	0,0043	0,0056	0,0062	0,0046	0,0039	0,0032	0,0025	0,0020	0,0016	0,0013	0,0012	
3	0,0007	0,0008	0,0010	0,0012	0,0015	0,0019	0,0027	0,0036	0,0043	0,0056	0,0062	0,0046	0,0039	0,0032	0,0025	0,0019	0,0016	0,0013	0,0011	
4	0,0007	0,0007	0,0009	0,0011	0,0015	0,0018	0,0026	0,0035	0,0041	0,0053	0,0060	0,0046	0,0039	0,0033	0,0026	0,0020	0,0016	0,0013	0,0012	
5	0,0007	0,0007	0,0009	0,0011	0,0014	0,0018	0,0025	0,0033	0,0040	0,0051	0,0057	0,0046	0,0040	0,0033	0,0027	0,0021	0,0017	0,0014	0,0012	
6	0,0007	0,0007	0,0009	0,0011	0,0014	0,0017	0,0024	0,0032	0,0038	0,0049	0,0055	0,0046	0,0040	0,0034	0,0028	0,0022	0,0017	0,0014	0,0012	
7	0,0007	0,0007	0,0009	0,0010	0,0014	0,0017	0,0023	0,0031	0,0037	0,0048	0,0053	0,0046	0,0041	0,0035	0,0028	0,0023	0,0018	0,0014	0,0013	
8	0,0007	0,0007	0,0009	0,0010	0,0013	0,0016	0,0022	0,0030	0,0036	0,0046	0,0051	0,0046	0,0041	0,0036	0,0029	0,0023	0,0019	0,0015	0,0013	
9	0,0007	0,0007	0,0009	0,0010	0,0013	0,0016	0,0021	0,0028	0,0034	0,0044	0,0050	0,0046	0,0041	0,0036	0,0030	0,0024	0,0019	0,0015	0,0013	
10	0,0007	0,0007	0,0008	0,0010	0,0013	0,0015	0,0021	0,0027	0,0033	0,0043	0,0048	0,0046	0,0041	0,0037	0,0031	0,0025	0,0019	0,0015	0,0014	
11	0,0007	0,0007	0,0008	0,0010	0,0012	0,0015	0,0020	0,0027	0,0032	0,0042	0,0046	0,0045	0,0042	0,0037	0,0031	0,0025	0,0020	0,0016	0,0014	
12	0,0007	0,0007	0,0008	0,0009	0,0012	0,0014	0,0020	0,0026	0,0031	0,0040	0,0045	0,0045	0,0042	0,0038	0,0032	0,0026	0,0020	0,0016	0,0014	
13	0,0007	0,0007	0,0008	0,0009	0,0012	0,0014	0,0019	0,0025	0,0030	0,0039	0,0044	0,0045	0,0042	0,0038	0,0033	0,0027	0,0021	0,0016	0,0014	
14	0,0007	0,0007	0,0008	0,0009	0,0011	0,0014	0,0019	0,0024	0,0029	0,0038	0,0042	0,0045	0,0042	0,0038	0,0033	0,0027	0,0021	0,0017	0,0015	
15	0,0007	0,0007	0,0008	0,0009	0,0011	0,0013	0,0018	0,0024	0,0028	0,0037	0,0041	0,0044	0,0042	0,0039	0,0034	0,0028	0,0021	0,0017	0,0015	
16	0,0007	0,0007	0,0008	0,0009	0,0011	0,0013	0,0018	0,0023	0,0027	0,0036	0,0040	0,0044	0,0042	0,0039	0,0035	0,0029	0,0022	0,0017	0,0015	
17	0,0007	0,0007	0,0008	0,0009	0,0011	0,0013	0,0017	0,0022	0,0026	0,0035	0,0039	0,0044	0,0042	0,0039	0,0035	0,0029	0,0022	0,0017	0,0015	
18	0,0007	0,0007	0,0008	0,0009	0,0011	0,0013	0,0017	0,0022	0,0026	0,0034	0,0038	0,0043	0,0042	0,0040	0,0036	0,0030	0,0023	0,0018	0,0016	
19	0,0007	0,0007	0,0007	0,0009	0,0010	0,0012	0,0016	0,0021	0,0025	0,0033	0,0038	0,0043	0,0042	0,0040	0,0036	0,0030	0,0023	0,0018	0,0016	
20	0,0007	0,0007	0,0007	0,0008	0,0010	0,0012	0,0016	0,0021	0,0025	0,0033	0,0037	0,0043	0,0042	0,0040	0,0036	0,0031	0,0023	0,0018	0,0016	
21	0,0007	0,0007	0,0007	0,0008	0,0010	0,0012	0,0016	0,0021	0,0024	0,0032	0,0036	0,0042	0,0042	0,0040	0,0037	0,0031	0,0024	0,0018	0,0016	
22	0,0007	0,0007	0,0007	0,0008	0,0010	0,0012	0,0015	0,0020	0,0024	0,0031	0,0035	0,0042	0,0042	0,0040	0,0037	0,0032	0,0024	0,0019	0,0016	
23	0,0007	0,0007	0,0007	0,0008	0,0010	0,0012	0,0015	0,0020	0,0023	0,0031	0,0035	0,0042	0,0042	0,0041	0,0037	0,0032	0,0024	0,0019	0,0016	
24	0,0007	0,0007	0,0007	0,0008	0,0010	0,0012	0,0015	0,0020	0,0023	0,0030	0,0034	0,0042	0,0042	0,0041	0,0038	0,0033	0,0024	0,0019	0,0017	
25	0,0007	0,0007	0,0007	0,0008	0,0010	0,0011	0,0015	0,0019	0,0023	0,0030	0,0034	0,0041	0,0042	0,0041	0,0038	0,0033	0,0025	0,0019	0,0017	
26	0,0007	0,0007	0,0007	0,0008	0,0010	0,0011	0,0014	0,0019	0,0022	0,0029	0,0033	0,0041	0,0042	0,0041	0,0038	0,0033	0,0025	0,0019	0,0017	
27	0,0007	0,0007	0,0007	0,0008	0,0010	0,0011	0,0014	0,0019	0,0022	0,0029	0,0033	0,0041	0,0042	0,0041	0,0038	0,0034	0,0025	0,0019	0,0017	
28	0,0007	0,0007	0,0007	0,0008	0,0009	0,0011	0,0014	0,0018	0,0022	0,0029	0,0032	0,0041	0,0042	0,0041	0,0039	0,0034	0,0025	0,0020	0,0017	
29	0,0007	0,0007	0,0007	0,0008	0,0009	0,0011	0,0014	0,0018	0,0022	0,0028	0,0032	0,0041	0,0042	0,0041	0,0039	0,0034	0,0025	0,0020	0,0017	
30	0,0007	0,0007	0,0007	0,0008	0,0009	0,0011	0,0014	0,0018	0,0021	0,0028	0,0032	0,0040	0,0042	0,0041	0,0039	0,0034	0,0026	0,0020	0,0017	
31	0,0007	0,0007	0,0007	0,0008	0,0009	0,0011	0,0014	0,0018	0,0021	0,0028	0,0031	0,0040	0,0042	0,0041	0,0039	0,0035	0,0026	0,0020	0,0017	
32	0,0007	0,0007	0,0007	0,0008	0,0009	0,0011	0,0014	0,0018	0,0021	0,0028	0,0031	0,0040	0,0042	0,0042	0,0039	0,0035	0,0026	0,0020	0,0017	
33	0,0007	0,0007	0,0007	0,0008	0,0009	0,0011	0,0014	0,0018	0,0021	0,0027	0,0031	0,0040	0,0042	0,0042	0,0039	0,0035	0,0026	0,0020	0,0017	
34	0,0007	0,0007	0,0007	0,0008	0,0009	0,0011	0,0014	0,0018	0,0021	0,0027	0,0031	0,0040	0,0042	0,0042	0,0039	0,0035	0,0026	0,0020	0,0018	
35	0,0007	0,0007	0,0007	0,0008	0,0009	0,0011	0,0014	0,0018	0,0021	0,0027	0,0031	0,0040	0,0042	0,0042	0,0039	0,0035	0,0026	0,0020	0,0018	

Table 18...continued. Geochemical modeling results for SiO₂ aqueous - test 14